nature cell biology

The Arp2/3 complex and WASp are required for apical trafficking of Delta into microvilli during cell fate specification of sensory organ precursors

Akhila Rajan[1,5,7], An-Chi Tien[2,6,7], Claire M. Haueter[3], Karen L. Schulze[3] and Hugo J. Bellen[1,2,3,4,8]

Cell fate decisions mediated by the Notch signalling pathway require direct cell–cell contact between adjacent cells. In *Drosophila melanogaster*, an external sensory organ (ESO) develops from a single sensory organ precursor (SOP) and its fate specification is governed by differential Notch activation. Here we show that mutations in *actin-related protein-3 (Arp3)* compromise Notch signalling, leading to a fate transformation of the ESO. Our data reveal that during ESO fate specification, most endocytosed vesicles containing the ligand Delta traffic to a prominent apical actin-rich structure (ARS) formed in the SOP daughter cells. Using immunohistochemistry and transmission electron microscopy (TEM) analyses, we show that the ARS contains numerous microvilli on the apical surface of SOP progeny. In *Arp2/3* and *WASp* mutants, the surface area of the ARS is substantially reduced and there are significantly fewer microvilli. More importantly, trafficking of Delta-positive vesicles from the basal area to the apical portion of the ARS is severely compromised. Our data indicate that WASp-dependent Arp2/3 actin polymerization is crucial for apical presentation of Delta, providing a mechanistic link between actin polymerization and Notch signalling.

Notch signalling is an evolutionarily conserved pathway used by metazoans to control cell fate decisions[1,2]. The Notch receptor and its ligands Delta and Serrate (Jagged in vertebrates) are single-pass transmembrane proteins. Cell–cell communication begins when the extracellular domain of the ligand on the signal-sending cell interacts with the extracellular domain of the Notch receptor on the signal-receiving cell. This interaction triggers a series of proteolytic cleavages that releases the intracellular domain of Notch, which enters the nucleus and functions as a transcriptional regulator[3].

Notch signalling mediates key decisions during nervous system development[4], including patterning and fate specification of the ESOs[5]. Each ESO is composed of four cell types (shaft, socket, sheath and neuron) and is derived from a single cell, the SOP (also called the pI cell), which is selected through Notch-mediated lateral inhibition at about 8–12 h after puparium formation (APF; Fig. 1a). The stage when the SOP has not yet undergone cell division is referred to as the 1-cell stage (15–18 h APF). During the 2-cell stage (~18–18.30 h APF) the SOP undergoes asymmetric cell division to generate the anterior pIIb and posterior pIIa (Fig. 1a). Because of the asymmetric distribution of cell fate determinants such as Numb and Neuralized[6,7], Notch signalling is differentially activated in pIIa and pIIb. The pIIa divides to create the external cells of the ESO, the shaft and socket cells. The pIIb divides twice to create the internal cells of the ESO, the neuron and sheath cell[8]. These four differentiated cells are collectively called the sensory cluster.

Delta and Serrate act redundantly to activate Notch during specification of pIIa and pIIb[9]. Recent studies indicate that endocytosis of Delta in the signal-sending cell is crucial for its ability to activate Notch[10]. An alternative, but not mutually exclusive model, is that ligand endocytosis promotes trafficking of the ligand to an endocytic recycling compartment, resulting in its activation[11,12]. In addition, apical trafficking of Delta seems to be important for proper fate specification in the SOP lineage[13]. However, the nature of ligand activation or the requirement for apical trafficking of the ligand remains unclear.

Here, we report that there is an apical actin-enriched structure in the pIIa and pIIb cells that contains numerous microvilli. The surface area of the actin-rich region and the number of microvilli are markedly reduced in *Arp2/3* complex and *WASp* mutants. More importantly, we found that the Arp2/3 complex and WASp have crucial roles in trafficking of endocytosed Delta vesicles to an apical ARS.

RESULTS

Mutations in *Arp3* result in a pIIa-to-pIIb cell fate transformation in *Drosophila* ESO lineages

Notch loss-of-function results in a pIIa-to-pIIb transformation, leading to loss of bristles[14]. Previous genetic screens based on assaying mitotic clones on the adult *Drosophila* thorax for bristle abnormalities[13,15,16] have

[1]Department of Molecular and Human Genetics, [2]Program in Developmental Biology, [3]Howard Hughes Medical Institute, [4]Department of Neuroscience, Baylor College of Medicine, Houston, TX 77030, USA. [5]Current address: Department of Genetics, Harvard Medical School, Boston, MA 021155, USA.[6]Current address: University of California, San Francisco, CA 94143, USA.
[7]These authors contributed equally to the work.
[8]Correspondence should be addressed to H.J.B. (e-mail: hbellen@bcm.tmc.edu)

Received 9 February 2009; accepted 17 March 2009; published online 21 June 2009; DOI: 10.1038/ncb1888

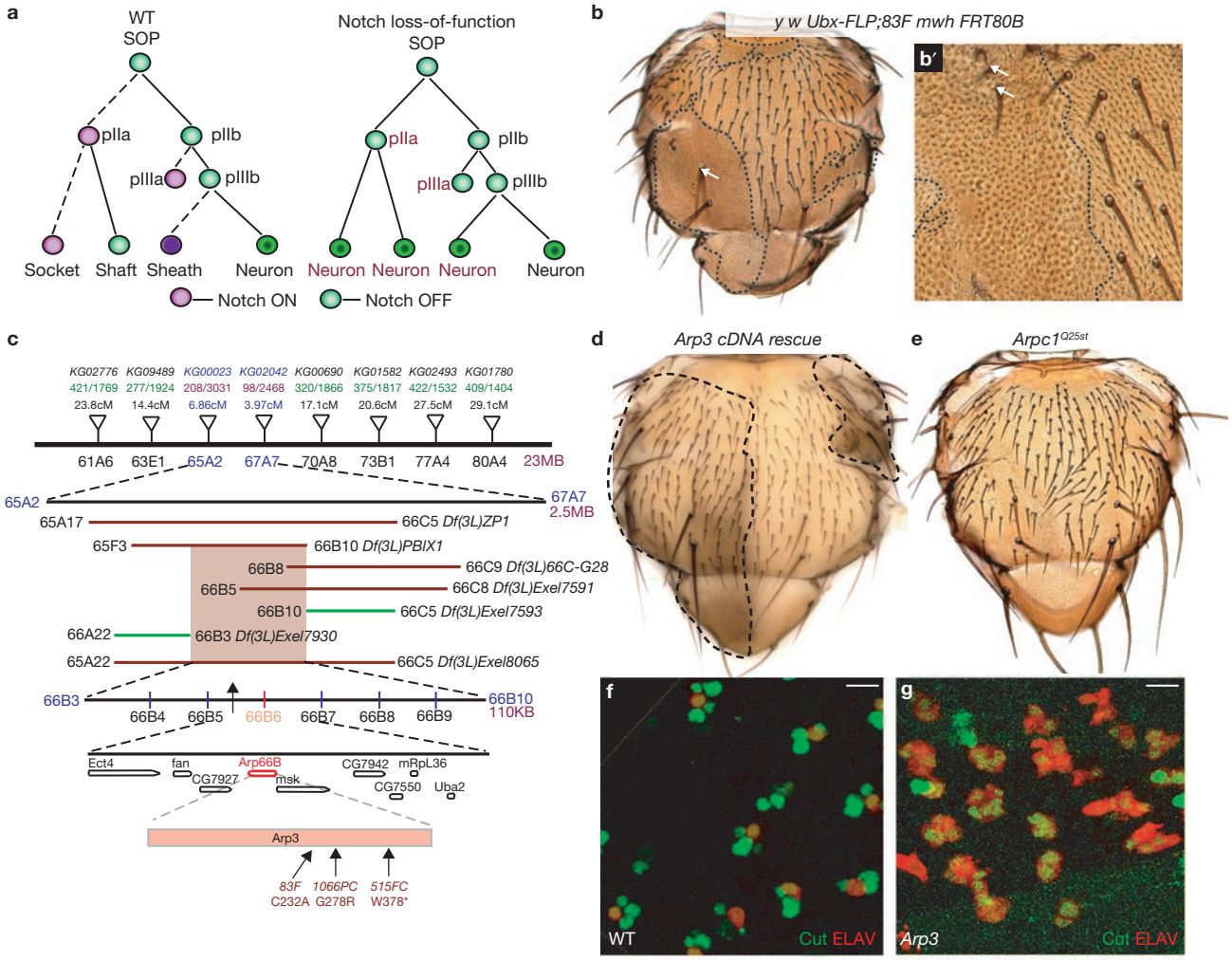

Figure 1 *Arp3* mutations cause a pIIa-to-pIIb transformation in the ESO lineage (**a**) A diagram of the ESO lineage in wild-type (WT) and in *Notch* loss-of-function background. Each cell is represented by a circle; the cells in which Notch is activated are in purple and the signal-sending cells are in green. The dashed lines indicate daughter cells in which Notch is activated. (**b**) Homozygous clones of $Arp3^{83F}$ on an adult thorax induced by *Ubx–FLP*. The clone (dashed lines) is identified by an epithelial cell marker *multiple wing hair (mwh)*, which marks the trichomes (small hair-like structures) on epithelial cells. Mutant clones show loss of external structures, socket and shaft cells, of the microchaetae. Macrochaetae (arrow) sometimes show a double-shaft phenotype in $Arp3^{83F}$ clones. (**b**′) Higher magnification of an $Arp3^{83F}$ clone shows that rarely there are shaft and sockets (arrows) in the mutant clone. Most of the $Arp3^{83F}$ clones show a balding phenotype. (**c**) Schematic representation of the mapping strategy. The inverted triangles represent *P* elements that were used for recombination mapping. Deficiencies represented by lines: those in red failed to complement the alleles, whereas those in green complement our alleles. (**d**) Rescue of the *Arp3* phenotype by overexpression of an *Arp3* cDNA construct in the mutant clones. An image of a pupal notum of an adult thorax which harbours *Arp3* clones; the mutant clones (dashed lines) do not show bristle loss (compare with **b**). (**e**) Flies that harbour clones of $Arpc1^{Q25st}$ show bald patches. The clones were not generated in a *Minute* background and hence appear smaller than *Arp3* clones (compare with **b**). We have not outlined the clones in $Arpc1^{Q25st}$ as they are unmarked clones. (**f**, **g**) A projection of confocal slices show part of the notum at 24–26 h APF stained for ELAV (red) and Cut (green). All cells in the wild-type (**f**) sensory clusters are positive for Cut and one of the cells is ELAV-positive. In *Arp3* (**g**) mutant clones all of the cells in the sensory clusters are positive for Cut and ELAV, indicating the transformation of all SOP progeny to neurons. Scale bar, 10 μm.

identified components in the Notch pathway[14]. We performed a similar F1 mitotic recombination screen on chromosome arm 3L[16] and isolated one complementation group consisting of three homozygous lethal alleles (*83F*, *515FC* and *1066PC*) that cause bristle loss in clones (Fig. 1b, b′). Using a recombination-based mapping strategy[17], the lethality of these alleles was mapped to the 66B cytological region (Fig. 1c). We obtained a *P* element *EP(3)3640* (ref. 18) inserted upstream of the *Arp3* gene that failed to complement our alleles, and identified molecular lesions in *Arp3* for the three alleles (Fig. 1c). Overexpression of the *Arp3* cDNA in *Arp3* mutant clones rescued the lethality and ESO phenotype (Fig. 1d), demonstrating that the observed phenotypes are caused by loss of *Arp3*.

Arp3 is part of the seven-protein Arp2/3 complex, which functions together for polymerization of branched actin filaments[19]. Another component of the Arp2/3 complex, Arpc1, was shown to be involved in ring canal formation during oogenesis in *Drosophila*[18]. As with *Arp3* alleles, $Arpc1^{Q25st}$ clones also cause bristle loss (Fig. 1e)[20]. Bristle loss in *Arp3* clones does not result from a failure to specify SOPs (Supplementary Information, Fig. S1a, a′). To examine whether bristle loss in *Arp3* clones is associated with a *Notch* loss-of-function defect, SOP progeny

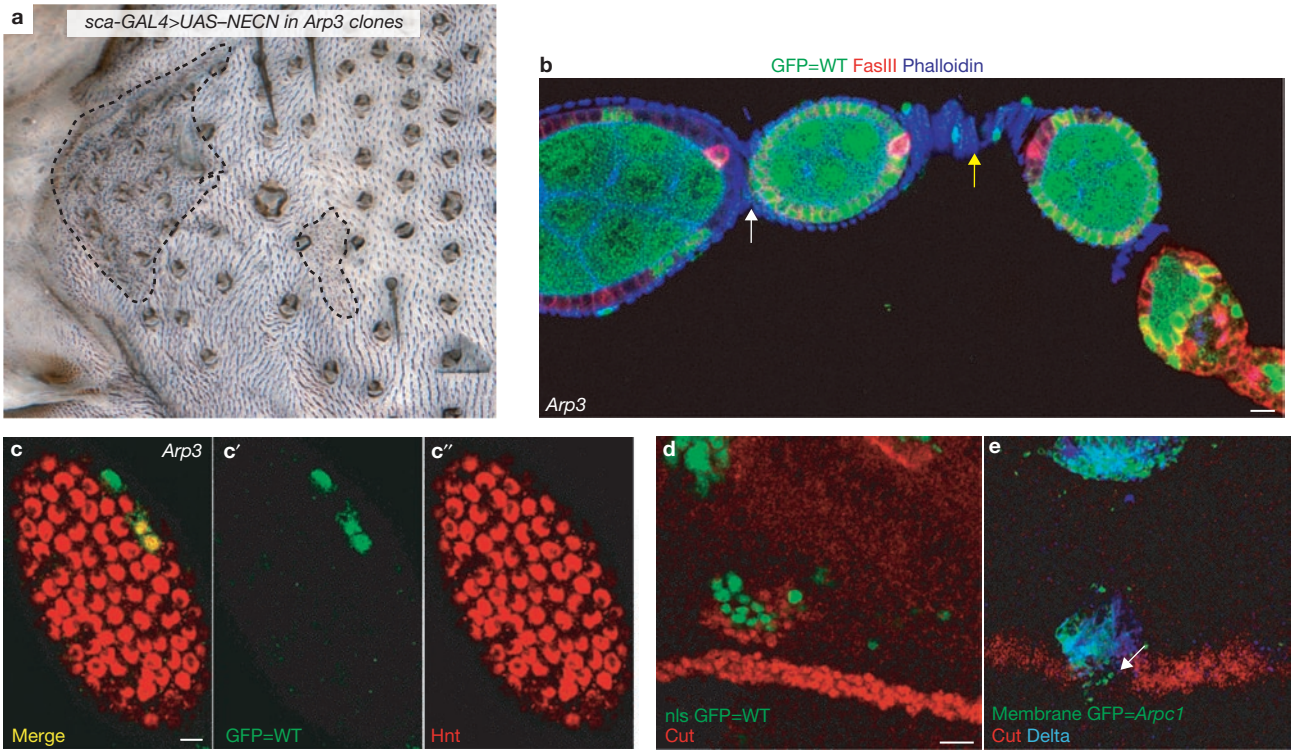

Figure 2 Arp3 is required in the signal sending cells during Notch signalling (**a**) Overexpression of N^{ECN} in wild-type SOPs using the sca^{109-68}-*GAL4* driver results in a multiple socket phenotype in the majority of the sensory clusters. We generated *Arp3* clones (dashed line) using *Ubx–FLP* in this N^{ECN} overexpression background. We did not observe a region of bald cuticle in the *Arp3* clones. (**b**) Clones of $Arp3^{515FC}$ induced by *hs-FLP* in follicle cells are marked by the absence of GFP (green). FasciclinIII (red) marks the follicle cells and is upregulated in polar follicle cells. Phalloidin (blue) marks the membrane of all cells. When polar follicle cells are wild-type (WT), stalk cells (yellow arrow) are formed normally, separating two cysts, whereas, when the polar follicle cells are mutant for *Arp3,* we found a loss of stalk cells between the cysts, resulting in a partial fusion of cysts (white arrow). (**c**–**c**′′) The follicle cells of the cyst harbour mutant clones of *Arp3* induced by *hs-FLP* at stage 7 of oogenesis. *Arp3* mutant clones are marked by the absence of nuclear GFP (green). The cyst was immunostained for Hnt (red), a Notch downstream target gene in the follicle cells. Note that Hnt is still expressed in the *Arp3* mutant follicle cell clones (non-green cells). (**d**) Overexpression of Delta in WT cells (green) near the dorsal-ventral boundary of the wing can induce Cut expression (red) in the adjacent cells near the dorsal-ventral boundary at the dorsal compartment. (**e**) Overexpression of Delta (blue) in *Arpc1* mutant cells (green) cannot induce Cut expression (red) in the adjacent cells near the dorsal-ventral boundary at the dorsal compartment. Note the loss of Cut expression when the clone crosses the dorsal-ventral boundary (arrow). Scale bars, 10 μm (**b**, **d**) and 5 μm (**c**).

at 24 h APF were labelled with differentiation markers. In wild-type sensory clusters, all four cells expressed the homeodomain protein Cut and one expressed the neuronal marker ELAV (Fig. 1f). In contrast, sensory clusters in both *Arp3* and $Arpc1^{Q25st}$ mutant clones contained 4–6 ELAV-positive cells (Fig. 1g and data not shown), suggesting that there is a pIIa-to-pIIb fate transformation.

Although a pIIa-to-pIIb transformation might result from disruption of asymmetric localization of cell fate determinants[6,7], both Neuralized and Numb were asymmetrically localized in *Arp3* mutant SOPs (Supplementary Information, Fig. S1c, e). One of the activators of the Arp2/3 complex, Wiskott-Aldrich syndrome protein (WASp)[21], is also involved in a similar fate specification process in *Drosophila*[22]. Together these observations suggest a specific requirement for WASp-regulated Arp2/3-complex function in Notch signalling.

Arp3 functions in the signal-sending cell during Notch signalling

Is Arp2/3 function required in the signal-sending or the signal-receiving cell during Notch signalling? We first determined the epistatic relationship between *Notch* and *Arp3* with a constitutively active Notch that is independent of ligand activation (N^{ECN})[23]. Expression of N^{ECN} in the ESO lineage causes a *Notch* gain-of-function phenotype, which results in generation of extra socket cells[13]. Overexpression of N^{ECN} in *Arp3* clones, as in wild-type cells, resulted in a *Notch* gain-of-function phenotype, indicating that a ligand-independent form of *Notch* is epistatic to *Arp3* (Fig. 2a). This places the function of Arp3 upstream of Notch activation, possibly in the signal-sending cell.

To gather evidence for a requirement of *Arp3* in the signal-sending cell, we examined its function in oogenesis. Egg chambers are individual units, consisting of germline cells surrounded by somatic follicle cells. The follicle cells can be further divided into three distinct populations: main body follicle cells (phalloidin-positive cells, Fig. 2b), which encapsulate the germline cyst; polar cells, which function as signalling centres (FasIII-positive cells, Fig. 2b); and stalk cells that connect neighbouring cysts (yellow arrow, Fig. 2b). The role of Notch signalling is well-documented in oogenesis[24,25], and signal-sending and receiving cells are spatially well-segregated. *Notch* loss-of-function causes the inability of the follicle cells to encapsulate germline cysts and leads to the formation of giant compound egg chambers[25]. However, *Delta* loss-of-function in follicle cells does not result in an encapsulation defect[25] but rather, loss of stalk cells and partial fusion of the cysts. Delta is required in the anterior polar follicle cells of the posterior egg chamber to specify stalk cells[25,26]. Generating follicle cell clones of *Notch* and *Delta*, therefore, results in

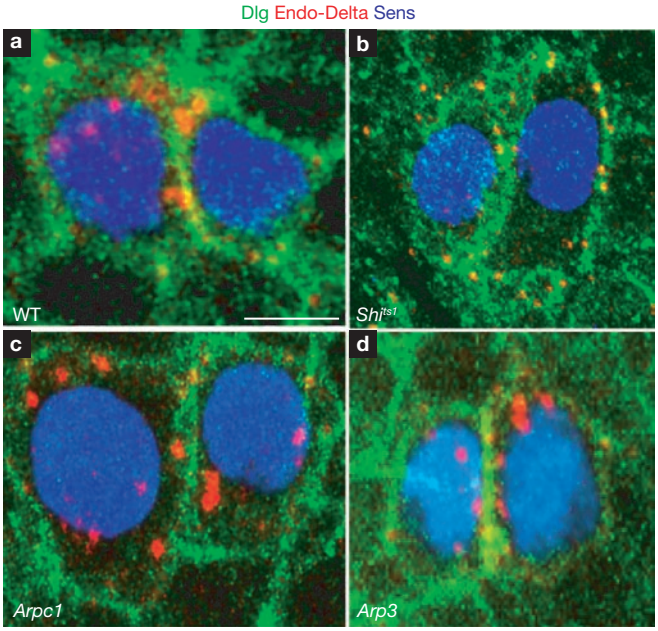

Figure 3 Delta is normally endocytosed in *Arp3* and *Arpc1* mutant pIIa-pIIb. (**a**–**d**) Endocytosis assay for Delta ligand (red) performed at the 2-cell stage in pIIa-pIIb. Sens (blue) labels the nucleus and Dlg (green) marks the sub-apical membrane. A projection of optical slices shows that in the negative control (*shi*^{ts1} (**b**), Delta (red) is found only on the membrane and not in cytoplasmic vesicles between the nucleus and membrane. However, in the wild-type (WT, **a**), *Arpc1* (**c**) and *Arp3* (**d**) pIIa-pIIb, endocytosed Delta vesicles (red) are present in the cytoplasm, indicating that Arp2/3 function is not required for Delta endocytosis. Note small punctae in **b** when Delta is not endocytosed. Scale bar, 5 μm.

distinct phenotypes. We found that loss of *Arp3* phenocopied loss-of-function of *Delta*. Mutant clones of *Arp3* ($n = 14$) in anterior polar follicle cells resulted in loss of stalk cells and partial fusion of adjacent cysts (white arrow, Fig. 2b). At later stages of oogenesis, Delta signals from the germ cells (signal-sending cells) activate Notch in the overlying somatic follicle cells (signal-receiving cells), resulting in expression of a Notch downstream target, Hindsight (Hnt)[27]. Arp3 does not seem to be required in the signal-receiving cell for Notch function, as expression of Hnt was normal in *Arp3* mutant follicle cell clones (Fig. 2c, c′).

To further examine whether Arp2/3 function is required in the signal-sending cell during wing formation, a Delta overexpression assay was performed. During wing development, pre-patterning signals, including Notch, are required to compartmentalize the immature wing imaginal disc at the third-instar larva[28]. Notch signalling is required to activate Cut expression at the dorsal-ventral boundary[29,30]. Previous studies have shown that overexpression of Delta in wild-type clones near the dorsal-ventral boundary results in ectopic Cut expression in the neighbouring cells (Fig. 2d)[11,16,29,30]. However, similar overexpression of Delta in *Arpc1* clones failed to activate Cut expression and resulted in loss of endogenous Cut expression when the clone crossed the dorsal-ventral boundary (Fig. 2e). These data suggest that Arp2/3 complex function is required for the normal function of Delta in the signal-sending cell.

The Arp2/3 complex is not required for Delta endocytosis

Delta must be endocytosed in the signal-sending cell to activate Notch on the receiving cell[6,31]. As Arp2/3 and WASp have been shown to be required for clathrin-mediated endocytosis in yeast[32,33], Arp2/3 might be required for Delta endocytosis during fate specification. However, by performing a Delta endocytosis assay[6] at the 2-cell stage, we found that Delta is endocytosed similarly to wild-type cells (Fig. 3a) in *Arpc1* and *Arp3* mutant tissue (Fig. 3c, d). By contrast, in *shibire* (*Dynamin*) mutant cells kept at the restrictive temperature (Fig. 3b), Delta is not endocytosed[34,35]. This indicates that the Arp2/3 complex is not required for ligand endocytosis during Notch signalling.

A specific ARS forms during fate specification in the ESO lineage

As Arp2/3 is required for polymerization of branched actin filaments[19], we visualized filamentous actin (F-actin) in the ESO lineage with phalloidin. In the wild-type, a prominent apical ARS was present in the pIIa and pIIb (pIIa-pIIb) cells (Fig. 4a, a′′). Co-staining of phalloidin and E-cadherin (*D*E-Cad), which highlights the apical-most stalk region of the pIIb cell that is engulfed by the pIIa cell[36], indicates that the ARS is present in both pIIa-pIIb cells apically (Supplementary Information, Fig. S1f, f′). However, no specialized apical actin enrichment was observed at the earlier 1-cell stage (Supplementary Information, Fig. S1g, g′). In *Arpc1* (yellow arrows, Fig. 4a, a′′), *Arp3* and *WASp* (data not shown) pIIa-pIIb cells, the ARS was formed. However, the apical area of the ARS was markedly reduced in *Arp3* (9.57 ± 5.32 μm^2; mean ± s.e.m, $n = 22$), *Arpc1* (12.25 ± 6.89 μm^2; $n = 19$) and *WASp* (21.86 ± 7.74 μm^2; $n = 19$) pIIa-pIIb cells when compared with the wild-type (43.48 ± 13.79 μm^2; Fig. 4b; $n = 18$). The ARS in wild-type pIIa-pIIb cells formed an umbrella shape along the *xy* axis, whereas in about 50% of the mutant ARS, the stalk of the umbrella was not formed properly (Fig. 4a′′, d).

To test whether the ARS is affected in other mutants, *α-Adaptin*[15] and *numb*[7], which regulate Notch signalling during pIIa-pIIb specification, were examined. In mutant clones of *α-Adaptin* (Fig. 4e) and *numb* (Fig. 4f) the ARS was formed normally, suggesting that the ARS defect is specific to *Arpc1*, *Arp3* and *WASp*. In *neuralized* clones, where both lateral inhibition and fate specification[37] are affected, the ARS was clearly observed in all SOP progeny (Fig. 4 g, g′′). This suggests that most, if not all, SOP progeny at the 2-cell stage are instructed to form an ARS.

To examine whether the Arp2/3 complex colocalizes with the ARS, we overexpressed a GFP-tagged *Arp3* cDNA construct (*UAS–Arp3–GFP)* by *neuralized–GAL4*. We observed that much of the GFP-tagged Arp3 protein colocalized with the ARS (Supplementary Information, Fig. S1h, h′′). The presence of the ARS in the pIIa-pIIb cells during fate specification and the fact that the ARS is morphologically affected in the *Arp3, Arpc1* and *WASp* mutants indicate that it has a role in Notch signal transduction.

Abundant actin-rich microvilli are present at the apical surface of pIIa-pIIb

The ARS was further analysed using TEM to visualize the actin cytoskeleton at the ultracellular level[38]. To distinguish the pIIa-pIIb cell-membrane from that of epithelial cells, HRP was overexpressed in the pIIa-pIIb cells using *neuralized–GAL4* and *UAS–CD2::HRP* (Fig. 5a). On DAB staining, HRP labelling was visualized as a darker cell membrane outline in the SOPs. The serial apical cross-sections (0–2520 nm) of the pIIa-pIIb cells revealed numerous membrane protrusions (Fig. 5b; Supplementary Information, Fig. S2). At high magnification (×10,000), we clearly observed actin bundles within these membranous extensions (Fig. 5c), which was confirmed by immuno-electron microscopy with phalloidin (Fig. 6a, a′). TEM analysis of *Arp3* pIIa-pIIb cells (Fig. 5d–f)

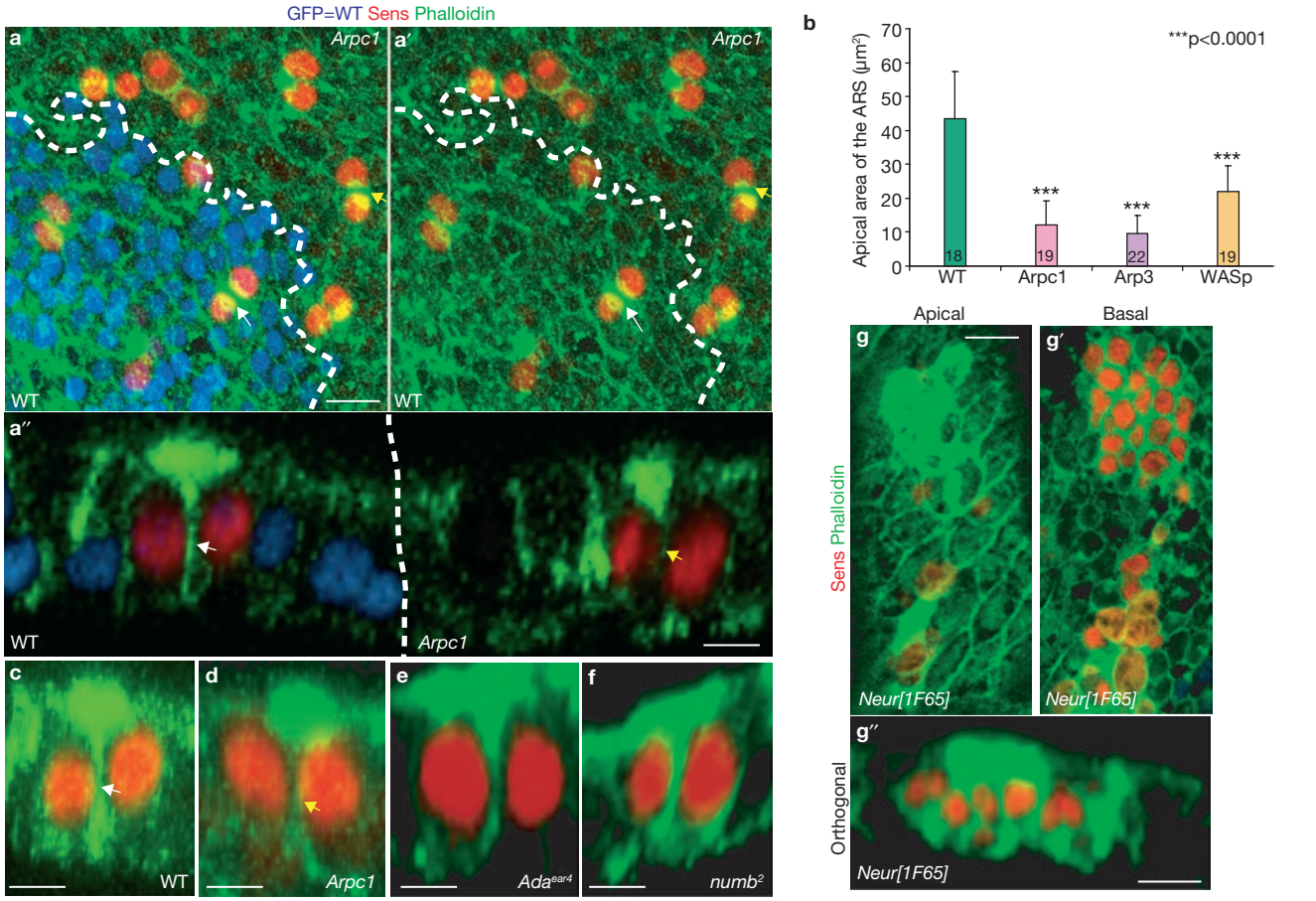

Figure 4 The ARS forms specifically in the pIIa-pIIb progeny and is reduced in *Arp3*, *Arpc1* and *WASp* mutant SOP progeny. (**a**, **a**′) A projection of confocal sections shows that the ARS identified by phalloidin (green) staining is present in both wild-type (WT, white arrow) pIIa-pIIb and *Arpc1* (yellow arrow) mutant pIIa-pIIb cells marked by Sens (red). *Arpc1* homozygous mutant clones (dotted lines) are marked by the absence of nuclear GFP (blue). (**a**′′) An orthogonal confocal section shows that the ARS is quite broad in the WT pIIa-pIIb (white arrow) and has an umbrella-shaped structure, whereas the ARS in the *Arpc1* homozygous clones (yellow arrow) seems compressed and the lateral 'stalk' of the ARS is malformed. (**b**) Quantification of the apical area of the ARS in different genotypes. The ARS area was quantified using the Measure function of ImageJ software. The measurements were analysed using a Student's *t*-test (***P <0.0001). Data are mean ± s.e.m. and the number of SOP progeny pairs used for quantification per genotype is indicated in the bars. (**c**–**g**′′) Pupal nota stained with Sens (red) and phalloidin (green) reveal ARS in pIIa-pIIb. Projections of orthogonal slices show the ARS in WT (**c**, white arrow), *Arpc1* (**d**, yellow arrow), *α-adaptin* (**e**), *numb* (**f**) and *neuralized* (**g**–**g**′′) pIIa-pIIb. An apical section (**g**) reveals apical (0.5 μm) actin enrichment whereas a basal section (**g**′) of the sample (~6 μm) shows the nuclei of the SOP progeny. Scale bars, 10 μm (**a**, **a**′′, **g**, **g**′′) and 5 μm (c–f).

revealed fewer finger-like projections than in wild-type cells (Fig. 5g), consistent with the marked reduction in apical surface area of the ARS in *Arp3*, *Arpc1* and *WASp* mutants (Fig. 4b). Finger-like projections were present on the epithelial cells, but there were fewer and they were markedly shorter (only about 60 nm in length), compared with those of pIIa-pIIb (Supplementary Information, Fig. S3a, c).

The finger-like actin projections on the pIIa-pIIb cells resemble microvilli, which are typically observed to be densely packed in intestinal and kidney epithelial cells[39], and circulating leukocytes[40]. Microvilli on the intestinal and kidney epithelial cells are thought to increase the surface area for absorption, whereas in leukocytes they have been implicated in receptor presentation, which enables leukocyte adhesion[41,42]. To examine whether the finger-like projections are microvilli, the ARS was immunostained with a microvilli marker myosin 1B (Myo1B), which forms lateral tethers between the microvillar membrane and underlying actin filament core[43]. We found that Myo1B is indeed enriched in the apical region of pIIa-pIIb cells (Fig. 6b, b′), specifically at the base of the 'umbrella' region of the ARS (Fig. 6b′′′). This localization of Myo1B was unaffected in *Arp3* mutant pIIa-pIIb cells (Supplementary Information, Fig. S3e, e′). These data indicate that microvilli are present on the apical region of pIIa-pIIb cells.

Delta traffics to the ARS

Intracellular vesicular trafficking of Delta is emerging as a key regulatory step in the activation of Notch[44,45]. We investigated Delta trafficking by co-staining of phalloidin and Delta. In wild-type pIIa-pIIb cells, Delta vesicles colocalized with the apical microvillar region of the ARS (Fig. 7a and transverse section in 7a′). In *Arpc1* (Fig. 7b and transverse section in Fig. 7b′) and *Arp3* (data not shown) pIIa-pIIb, fewer Delta vesicles were colocalized with the ARS. Furthermore, when serial sections were projected to visualize the whole cell (Fig. 7c, c′′), the Delta vesicles were clustered close to the wild-type ARS, whereas the vesicles were widely distributed in the cytoplasm of *Arpc1* pIIa-pIIb cells. The marked reduction of Delta vesicles colocalizing with the ARS in the mutant pIIa-pIIb cells suggests that Arp2/3 has a role in Delta trafficking to the ARS.

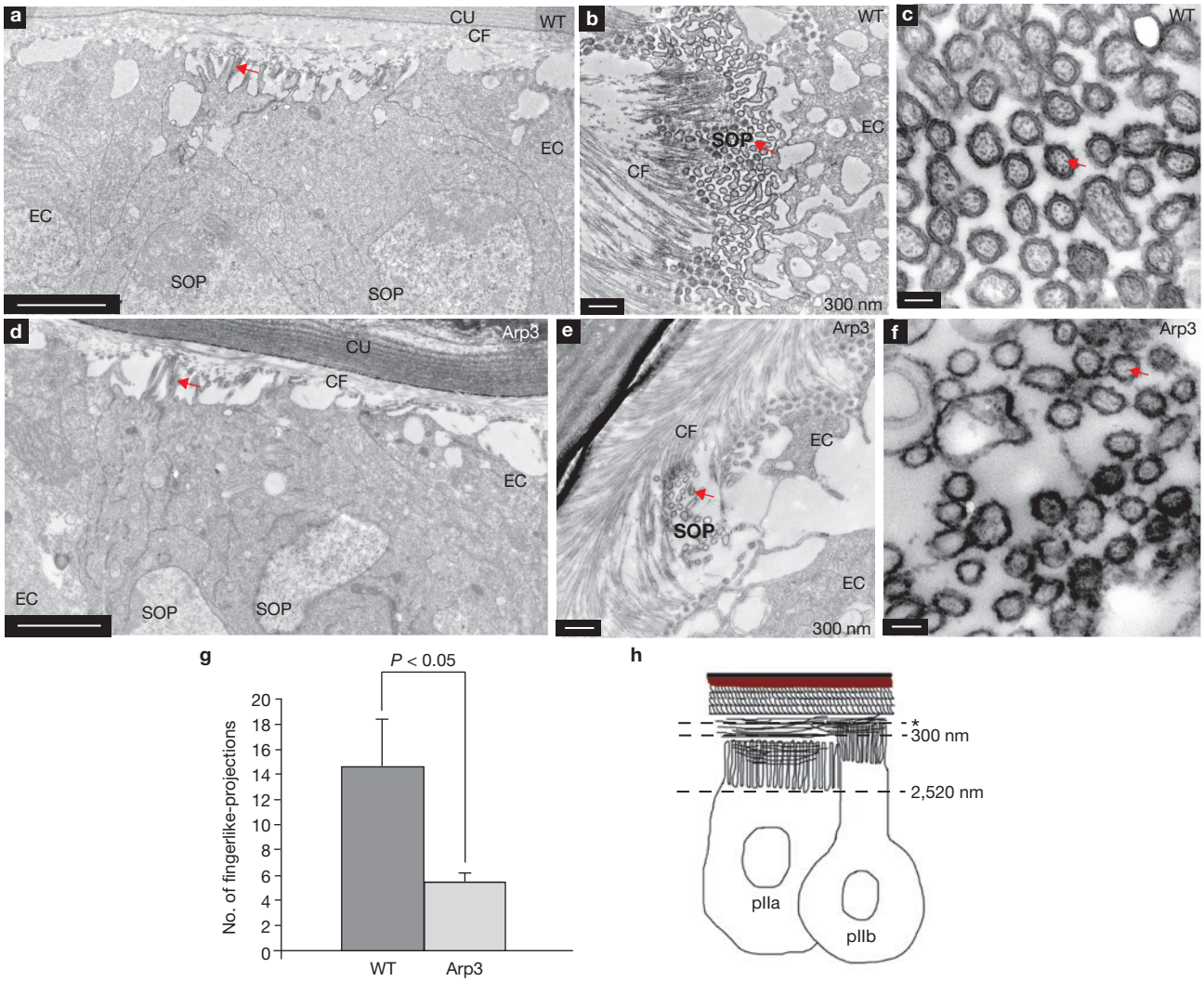

Figure 5 TEM analysis reveals enrichment of actin-filled finger-like projections in pIIa-pIIb cells at 18 h APF. (**a**, **d**) Orthogonal sections of wild-type (WT, **a**) and *Arp3* (**d**) pIIa-pIIb cells show finger-like projections (arrows) at the apical domain of the cells. (**b**–**f**) Cross-section of WT (**b**) and *Arp3* (**e**) pIIa-pIIb cells show finger-like projections (arrows). (**c**, **f**) Higher magnification of the apical surface of WT (**c**) and *Arp3* (**f**) pIIa-pIIb cells shows actin bundles (arrows) inside the finger-like projections. (**g**) Quantification of the number of finger-like projections at the 2-cell stage in WT and *Arp3*. The total number of microvilli in SOP and epithelial cells were quantified using ImageJ. The data are mean ± s.e.m and measurements were analysed using Student's *t*-test. Three SOP progeny pairs were used for this quantification per genotype. (**h**) Schematic representation of pIIa-pIIb in the prepupal thorax epithelium. The asterisk represents the level of the first electron microscopy section at 60 nm. Abbreviations: cuticle (Cu), chitin fibre (CF), epithelial cell (EC), sensory organ precursor cell (SOP). Scale bars, 0.5 μm (**a**, **b**, **d**, **e**) and 0.1 μm (**c**, **f**).

Arp2/3 and WASp are required for trafficking of endocytosed Delta to the apical ARS

To investigate Delta trafficking in *Arp2/3* and *WASp* mutants, we performed pulse-chase labelling experiments[12] to monitor the internalization of Delta in living pupae. Internalization of Delta vesicles with respect to ARS was examined at three different time-points (0, 30 and 60 min). At 0 min Delta vesicles were present apically (~0.5 μm into the sample) and colocalized with ARS in wild-type (Fig. 8a, a′′), *Arp3* (Fig. 8b, b′′), *Arpc1* and *WASp* (data not shown) SOP progeny. At 30 min post-internalization, Delta vesicles were localized basally (~6 μm) in wild-type (Fig. 8c, c′′) and *Arp3* (Fig. 8d, d′′) SOP progeny, indicating that the Delta vesicles had trafficked intracellularly at this time-point. However, 60 min after internalization, localization of Delta vesicles in mutants differed from the wild-type. In the wild-type, about 6–10 Delta-positive vesicles colocalized apically on the ARS (Fig. 8e, e′′), suggesting that endocytosed Delta traffics back to the apical microvilli. In *Arp3* (Fig. 8f, f′′), *Arpc1* (Supplementary Information, Fig. S4a, a′′) and *WASp* (Supplementary Information, Fig. S4b, b′′) mutants, Delta vesicles were not localized apically on the ARS. Instead, they were found basally in the cytoplasm (~6 μm into the cell; Fig. 8f′, f′′; Supplementary Information, Fig. S4a′–b′′), suggesting a defect in Delta trafficking. Indeed, the number of Delta vesicles that traffic to the microvillar region of the ARS at 60 min post-chase was significantly lower in the *Arpc1*, *Arp3* and *WASp* pIIa-pIIb than in wild-type cells (Fig. 8g). However, the total number of internalized Delta vesicles and the intensity of Delta signal in the SOP progeny at 60 min post-chase were very similar in wild-type and mutants (Supplementary Information, Fig. S4c, d). In summary, initially Delta is properly targeted apically at the ARS and endocytosed (Fig. 8a–b′′). Delta traffics basally in both wild-type and mutants (Fig. 8c–d′′) 30

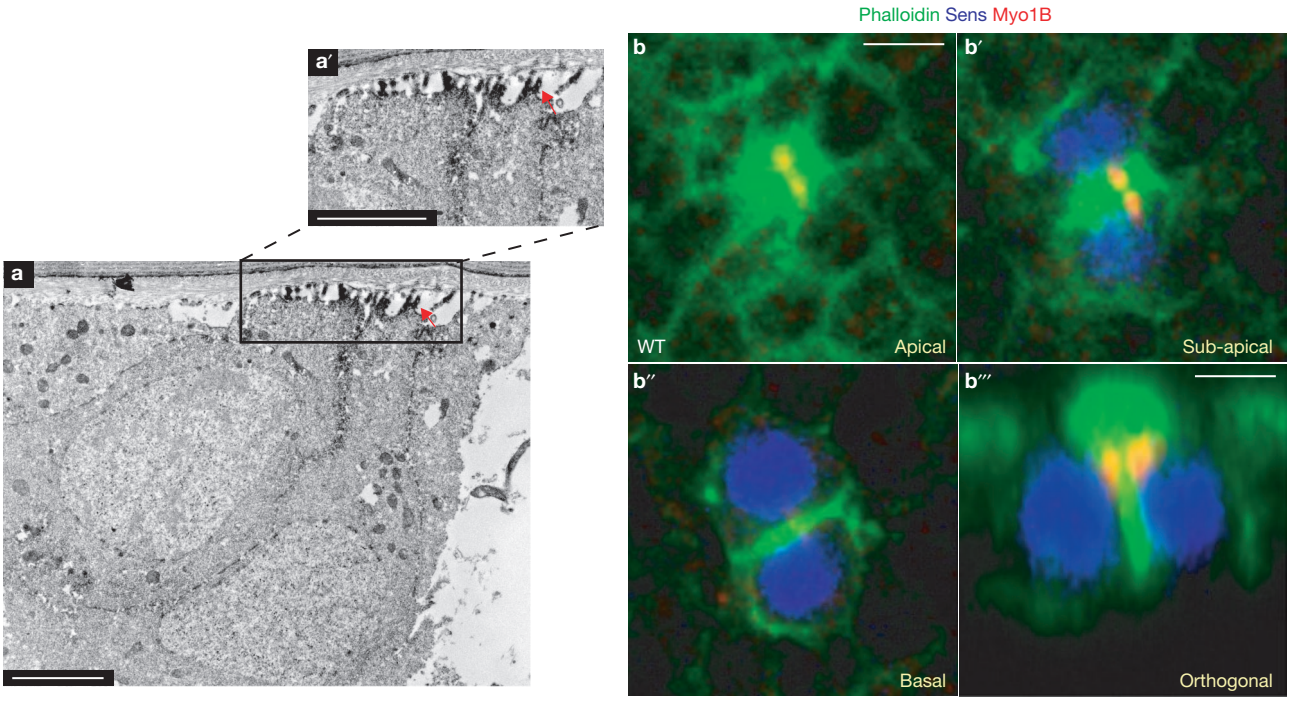

Figure 6 Finger-like projections in pIIa-pIIb cells are enriched with F-actin bundles and are marked by a microvillar marker Myo1B. (**a**, **a**′) Immuno-electron microscopy image of an orthogonal section through the wild-type pIIa-pIIb of a pupal notum shows an enrichment of phalloidin (electron-dense material) in the finger-like projections along the apical region of the ARS. (**a**′) A higher magnification view of the boxed region in **a** is shown in **a**′. The arrow points to the enrichment of phalloidin in the finger-like projections (**b**–**b**‴) Confocal images of single optical (*xy* axis) sections (**b**–**b**″) and orthogonal section (**b**‴) of wild-type (WT) pIIa-pIIb cells immunostained for Myo1B (red), phalloidin (green) and Sens (blue). Scale bars, 0.5 μm (**a**, **a**′) and 5 μm (**b**, **b**‴).

min after internalization. However, endocytosed Delta is not targeted back to the microvillar region in *Arp3*, *Arpc1* and *WASp* SOP progeny 60 min post-chase.

It has been proposed that Delta must be endocytosed and targeted to a specific endosomal compartment to become activated[11], possibly through Rab11-positive recycling endosomes[12,13]. By examining the distribution of the vesicular compartments, we found that the early endosome and the recycling endosome were enriched on the ARS (Supplementary Information, Fig. S4e–h′). Pulse-chase of endocytosed Delta through these compartments (Supplementary Information, Figs S5, S6), showed no significant defects in the localization and abundance of these endosomal compartments or the ability of Delta to traffic through these endosomal compartments in *Arpc1* mutant SOP progeny. The internalized Delta is thought to be proteolytically cleaved in an unknown compartment[11]. We found that Delta processing in *Arp3* mutants is similar to that in the wild-type (Supplementary Information, Fig. S7).

In summary, we surmise that a defect in trafficking of endocytosed Delta to the apical microvillar portion of the ARS leads to a failure in Delta signalling. We conclude that this defect underlies the pIIa-to-pIIb fate transformation phenotype in *Arp3, Arpc1* and *WASp* mutants.

DISCUSSION

Previous reports have suggested that trafficking of a subset of endocytosed Delta to the apical membrane in the pIIb cell is required for its ability to activate Notch in the pIIa cell[12,13]. We have uncovered a highly stereotyped ARS that consists of apical microvilli and a lateral 'stalk' region. In *Arp2/3* and *WASp* pIIa-pIIb cells, the apical surface area of the ARS was significantly reduced and the number of microvilli on the apical region was also reduced. In addition, trafficking of endocytosed Delta to the apical microvilli-rich region of the ARS was severely impaired in *Arp3* mutants. Although numerous studies have focused on the SOP daughter cells, the ARS and the microvilli have not been described previously. These microvillar structures are very different from filopodia[46], which have been reported to have a role in lateral inhibition[47] at an earlier stage. Our data indicate that apical trafficking of Delta to the ARS is required for its ability to signal.

Given the role of Arp2/3 in forming branched actin filaments, one of the primary roles of the Arp2/3 complex and WASp during Notch signalling is probably to form actin networks[48], and to enable and/or to promote the trafficking of Delta vesicles to the ARS (Fig. 8h). This requirement for endocytosed Delta localization to the microvilli during Notch signalling is akin to findings showing that localization of Smoothened to primary cilia is important for its activation during Hedgehog (Hh) signal transduction[49,50]. An interesting study performed in circulating lymphocytes has demonstrated a crucial requirement for microvillar receptor presentation in leukocyte adhesion to the endothelial membrane[41]. In an analogous manner to findings in leukocytes, microvillar presentation of Delta might enhance its ability to contact Notch on the surface of the adjacent cell. As Notch signalling is a major contact-dependent signalling pathway, microvilli might therefore increase the surface area of contact between the signal-sending and receiving cells, enhancing the ability of the ligand to interact with the receptor.

On the basis of the well-characterized role for WASp and Arp2/3 in clathrin-mediated endocytosis[32], it was speculated that Arp2/3 and

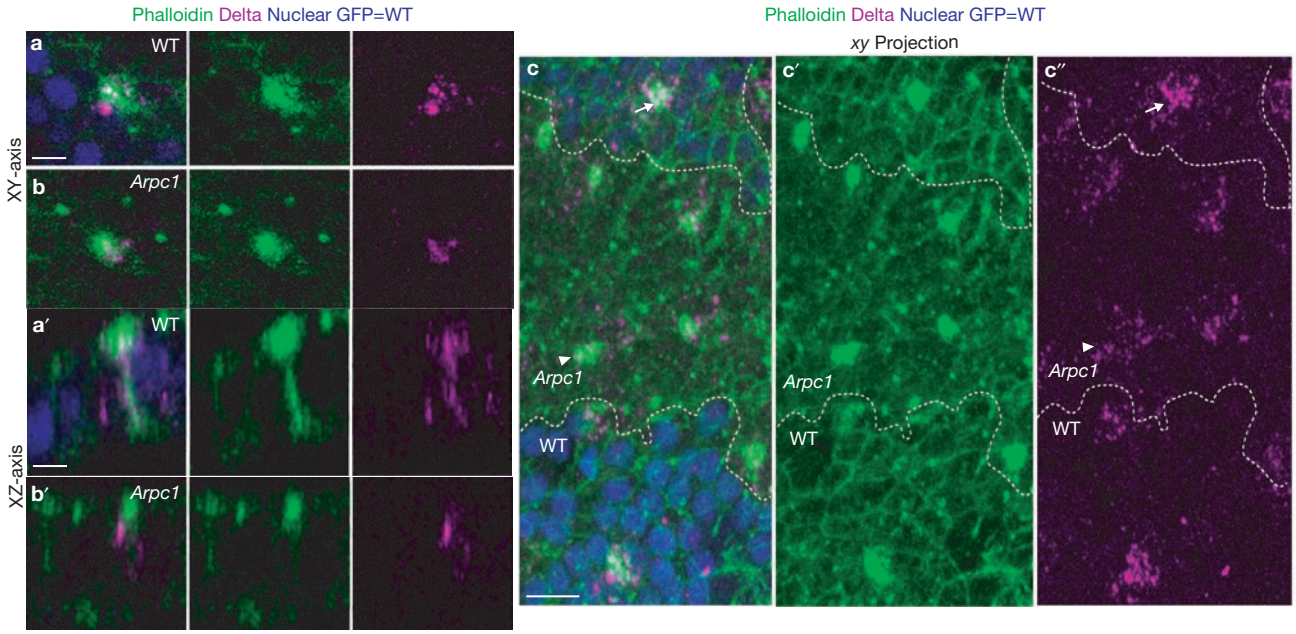

Figure 7 Delta localization to the ARS is reduced in *Arpc1* mutants. (**a**–**c**′′) Pupal wing nota at the 2-cell SOP stage (18.30 h APF) were immunostained with phalloidin (green) and Delta (magenta). *Arpc1* homozygous mutant cells are marked by the absence of GFP (blue). (**a**, **b**) A single section along the *xy* axis through pIIa-pIIb cells shows an enrichment of Delta on the ARS in wild-type (WT, **a**) and this enrichment is much reduced in *Arpc1* (**b**). (**a**′, **b**′) A single section along the *xy* axis of pIIa-pIIb shows that the Delta vesicles colocalize along the lateral stalk of the ARS in WT and in the basal portion of the umbrella region of the ARS (**a**′). In *Arpc1* (**b**′), the lateral stalk of the ARS is malformed and there is a reduction in the number of Delta vesicles that colocalize on the apical portion of the ARS. (**c**–**c**′′) A projection of confocal sections of a pupal notum harbouring an *Arpc1* mutant clone (dashed line). In the WT region, a high density of Delta vesicles are clustered on and around the ARS, whereas in the mutant clones, the Delta vesicles are more widely distributed and do not cluster around the ARS; compare arrowheads (*Arpc1*) with arrows (WT). Scale bars, 5 μm (**a**, **a**′) and 10 μm (**c**).

WASp might be required for endocytosis of Delta and/or Notch during signalling[51]. However, our data indicate that the Arp2/3 complex is not required for Notch in the signal-receiving cell. Our data also indicate that the Arp2/3 complex is not required to endocytose Delta. It is possible that endocytosis of Delta occurs in a clathrin-independent manner[52,53].

The involvement of *WASp* during Notch-mediated fate decisions might have implications for its mammalian homologue in Wiskott-Aldrich syndrome, an X-linked immunodeficiency[54]. Given that Notch signalling is required for proper T-cell development[55] and differentiation of peripheral T-cells[56], defects in Delta trafficking caused by WASp-mediated actin polymerization might underlie the loss and aberrant function of T cells in patients with Wiskott-Aldrich syndrome. Interestingly, microvilli on the surface of lymphocytes might also have a central role in receptor presentation in macrophages and T cells[41,42]. It will be interesting to investigate whether WASp has a role in Notch signalling during T-cell development and activation. □

METHODS

Methods and any associated references are available in the online version of the paper at http://www.nature.com/naturecellbiology/

Note: Supplementary Information is available on the Nature Cell Biology website.

ACKNOWLEDGEMENTS

We are grateful to W. Theurkauf, L. Cooley, E. Schejter, J. Skeath, D. F. Ready, P. Badenhorst, Y. N. Jan, P. Bryant, M. González Gaitán, G. Struhl, E. C. Lai, M. Muskavitch, A. L. Parks, F. B. Gertler, L. M. Lanier, J. Knoblich, F. Schweisguth, R. Dubreuil, W. Sullivan, M. S. Mooseker, G.M. Guild, the Bloomington Stock Center and the Developmental Studies Hybridoma Bank for reagents. We thank G. Emery for advice regarding the Delta endocytosis assay. We would like to thank H. Jafar-Nejad for suggestions and advice during the screen and comments on the manuscript. We thank P. Verstreken and C. V. Ly for their help with the screen, and R. Atkinson for advice on imaging. Confocal microscopy was supported by the BCM Mental Retardation and Developmental Disabilities Research Center. H.J.B. is an investigator of the Howard Hughes Medical Institute.

AUTHOR CONTRIBUTIONS

A.R., A.T. and H.B. conceived the project. A.R. and A.T. carried out the screen, mapped the genes and executed the project. K.S. was involved in the screen and mapping of the genes. C.M.H. in collaboration with A.R. and A.T. designed the TEM experiments and C.M.H. carried out the TEM experiments.

COMPETING INTERESTS

The authors declare that they have no competing financial interest.

Published online at http://www.nature.com/naturecellbiology/Reprints and permissions information is available online at http://npg.nature.com/reprintsandpermissions/

1. Tien, A. C., Rajan, A. & Bellen, H. J. A Notch updated. *J. Cell Biol.* **184 (5),** 621–629 (2009).
2. Bray, S. J. Notch signalling: a simple pathway becomes complex. *Nature Rev. Mol. Cell Biol.* **7,** 678–689 (2006).
3. Schweisguth, F. Regulation of Notch signaling activity. *Curr. Biol.* **14,** R129–138 (2004).
4. Louvi, A. & Artavanis-Tsakonas, S. Notch signalling in vertebrate neural development. *Nature Rev.* **7,** 93–102 (2006).
5. Bray S. Notch signalling in *Drosophila*: three ways to use a pathway. *Sem. Cell Dev. Biol.* **9,** 591–597 (1998).
6. Le Borgne, R. & Schweisguth, F. Unequal segregation of Neuralized biases Notch activation during asymmetric cell division. *Dev. Cell* **5,** 139–148 (2003).
7. Rhyu, M. S., Jan, L. Y. & Jan, Y. N. Asymmetric distribution of numb protein during division of the sensory organ precursor cell confers distinct fates to daughter cells. *Cell* **76,** 477–491 (1994).
8. Gho, M., Bellaiche, Y. & Schweisguth, F. Revisiting the *Drosophila* microchaete lineage: a novel intrinsically asymmetric cell division generates a glial cell. *Development* **126,** 3573–3584 (1999).
9. Zeng, C., Younger-Shepherd, S., Jan, L. Y. & Jan, Y. N. Delta and Serrate are redundant Notch ligands required for asymmetric cell divisions within the *Drosophila* sensory organ lineage. *Genes Dev.* **12,** 1086–1091 (1998).

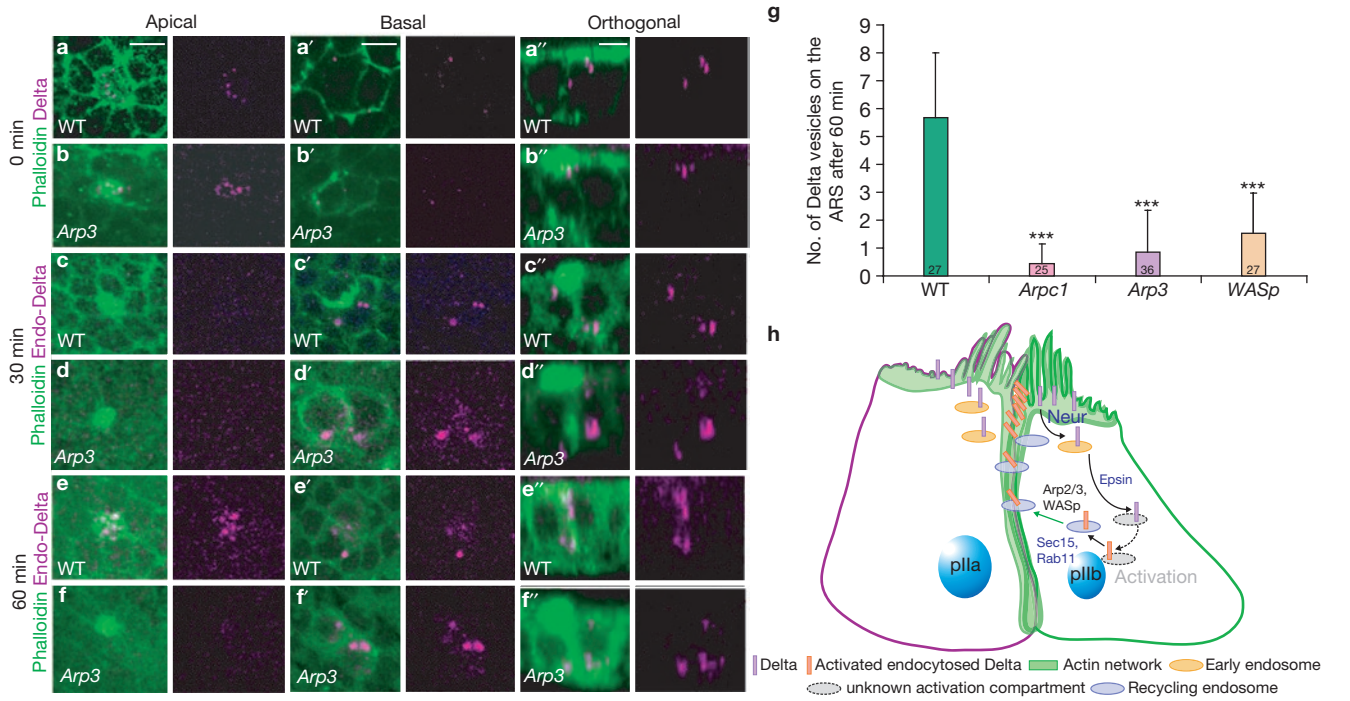

Figure 8 Arp2/3 and WASp are required for trafficking of endocytosed Delta to the apical ARS 1 h post-endocytosis. (**a**–**f**′′) A pulse-chase assay for the trafficking of endocytosed Delta (magenta) at different time-points with respect to the ARS (green) was performed in live pupal nota of wild-type (WT) and *Arp3* mutants. Confocal images show apical (0.5 μm), basal (6 μm) and orthogonal sections of the pIIa-pIIb cells of the WT notum (**a**–**a**′′, **c**–**c**′′, **e**–**e**′′), and *Arp3* mutant clones (**b**–**b**′′, **d**–**d**′′, **f**–**f**′′). The pulse-chase assays for three different time-points, 0 min, 30 min and 60 min, are shown. (**g**) Quantification of the number of internalized Delta vesicles that are present apically and colocalize with the ARS. Measurements of total number of Delta vesicles that traffic to the ARS 1 h after chase were analysed using a Student's *t*-test (***$P < 0.0001$). Data are mean ± s.e.m. and the number of SOP progeny pairs quantified per genotype is indicated in the bars. Note that fewer vesicles that colocalize in mutants when compared with the WT control and the difference is statistically significant. (**h**) Proposed model. In the pIIb cell, Delta is endocytosed by Neuralized (Neur)[6] and trafficked by Epsin[11] to an endocytic compartment where it undergoes activation, probably by a proteolytic cleavage event. It is trafficked back to the membrane in a compartment positive for Rab11 (ref. 12) and the exocyst complex member Sec15 (ref. 13). Arp2/3 and WASp are required for the formation of branched actin networks to form the 'stalk' of the ARS and enables endocytosed vesicles containing activated Delta to traffic back to the dense actin-rich microvilli at the apical membrane of the pIIb cell, where it can signal. Scale bars, 5 μm.

10. Parks, A. L., Klueg, K. M., Stout, J. R. & Muskavitch, M. A. Ligand endocytosis drives receptor dissociation and activation in the Notch pathway. *Development* **127,** 1373–1385 (2000).
11. Wang, W. & Struhl, G. *Drosophila* Epsin mediates a select endocytic pathway that DSL ligands must enter to activate Notch. *Development* **131,** 5367–5380 (2004).
12. Emery, G. *et al.* Asymmetric Rab 11 endosomes regulate delta recycling and specify cell fate in the *Drosophila* nervous system. *Cell* **122,** 763–773 (2005).
13. Jafar-Nejad, H. *et al.* Sec15, a component of the exocyst, promotes notch signaling during the asymmetric division of *Drosophila* sensory organ precursors. *Dev. Cell* **9,** 351–363 (2005).
14. Hartenstein, V. & Posakony, J. W. A dual function of the Notch gene in *Drosophila* sensillum development. *Dev. Biol.* **142,** 13–30 (1990).
15. Berdnik, D., Torok, T., Gonzalez-Gaitan, M. & Knoblich, J. A. The endocytic protein α-Adaptin is required for numb-mediated asymmetric cell division in *Drosophila*. *Dev. Cell* **3,** 221–231 (2002).
16. Tien, A. C. *et al.* Ero1L, a thiol oxidase, is required for Notch signaling through cysteine bridge formation of the Lin12-Notch repeats in *Drosophila melanogaster*. *J. Cell Biol.* **182,** 1113–1125 (2008).
17. Zhai, R. G. *et al.* Mapping *Drosophila* mutations with molecularly defined P element insertions. *Proc. Natl Acad. Sci. USA* **100,** 10860–10865 (2003).
18. Hudson, A. M. & Cooley, L. A subset of dynamic actin rearrangements in *Drosophila* requires the Arp2/3 complex. *J. Cell Biol.* **156,** 677–687 (2002).
19. Machesky, L. M. & Gould, K. L. The Arp2/3 complex: a multifunctional actin organizer. *Curr. Opin. Cell Biol.* **11,** 117–121 (1999).
20. Tal, T., Vaizel-Ohayon, D. & Schejter, E. D. Conserved interactions with cytoskeletal but not signaling elements are an essential aspect of *Drosophila* WASp function. *Dev. Biol.* **243,** 260–271 (2002).
21. Machesky, L. M. & Insall, R. H. Scar1 and the related Wiskott-Aldrich syndrome protein, WASP, regulate the actin cytoskeleton through the Arp2/3 complex. *Curr. Biol.* **8,** 1347–1356 (1998).
22. Ben-Yaacov, S., Le Borgne, R., Abramson, I., Schweisguth, F. & Schejter, E. D. Wasp, the *Drosophila* Wiskott-Aldrich syndrome gene homologue, is required for cell fate decisions mediated by Notch signaling. *J. Cell Biol.* **152,** 1–13 (2001).
23. Struhl, G., Fitzgerald, K. & Greenwald, I. Intrinsic activity of the Lin-12 and Notch intracellular domains *in vivo*. *Cell* **74,** 331–345 (1993).
24. Ruohola, H. *et al.* Role of neurogenic genes in establishment of follicle cell fate and oocyte polarity during oogenesis in *Drosophila*. *Cell* **66,** 433–449 (1991).
25. Lopez-Schier, H. & St Johnston, D. Delta signaling from the germ line controls the proliferation and differentiation of the somatic follicle cells during *Drosophila* oogenesis. *Genes Dev.* **15,** 1393–1405 (2001).
26. Assa-Kunik, E., Torres, I. L., Schejter, E. D., Johnston, D. S. & Shilo, B. Z. *Drosophila* follicle cells are patterned by multiple levels of Notch signaling and antagonism between the Notch and JAK/STAT pathways. *Development* **134,** 1161–1169 (2007).
27. Sun, J. & Deng, W. M. Hindsight mediates the role of notch in suppressing hedgehog signaling and cell proliferation. *Dev. Cell* **12,** 431–442 (2007).
28. de Celis, J. F., Garcia-Bellido, A. & Bray, S. J. Activation and function of Notch at the dorsal-ventral boundary of the wing imaginal disc. *Development* **122,** 359–369 (1996).
29. de Celis, J. F. & Bray, S. Feed-back mechanisms affecting Notch activation at the dorsoventral boundary in the *Drosophila* wing. *Development* **124,** 3241–3251 (1997).
30. Micchelli, C. A., Rulifson, E. J. & Blair, S. S. The function and regulation of cut expression on the wing margin of *Drosophila*: Notch, Wingless and a dominant negative role for Delta and Serrate. *Development* **124,** 1485–1495 (1997).
31. Seugnet, L., Simpson, P. & Haenlin, M. Requirement for dynamin during Notch signaling in *Drosophila* neurogenesis. *Dev. Biol.* **192,** 585–598 (1997).
32. Kaksonen, M., Toret, C. P. & Drubin, D. G. A modular design for the clathrin- and actin-mediated endocytosis machinery. *Cell* **123,** 305–320 (2005).
33. Galletta, B. J., Chuang, D. Y. & Cooper, J. A. Distinct roles for Arp2/3 regulators in actin assembly and endocytosis. *PLoS Biol.* **6,** e1 (2008).
34. Chen, M. S. *et al.* Multiple forms of dynamin are encoded by *shibire*, a *Drosophila* gene involved in endocytosis. *Nature* **351,** 583–586 (1991).
35. van der Bliek, A. M. & Meyerowitz, E. M. Dynamin-like protein encoded by the *Drosophila shibire* gene associated with vesicular traffic. *Nature* **351,** 411–414 (1991).
36. Le Borgne, R., Bellaiche, Y. & Schweisguth, F. *Drosophila* E-cadherin regulates the orientation of asymmetric cell division in the sensory organ lineage. *Curr. Biol.* **12,** 95–104 (2002).
37. Lai, E. C. & Rubin, G. M. neuralized functions cell-autonomously to regulate a subset of notch-dependent processes during adult *Drosophila* development. *Dev. Biol.* **231,** 217–233 (2001).

38. Maupin, P. & Pollard, T. D. Improved preservation and staining of HeLa cell actin filaments, clathrin-coated membranes, and other cytoplasmic structures by tannic acid-glutaraldehyde-saponin fixation. *J. Cell Biol.* **96,** 51–62 (1983).
39. Heintzelman, M. B. & Mooseker, M. S. Assembly of the intestinal brush border cytoskeleton. *Curr. Top. Dev. Biol.* **26,** 93–122 (1992).
40. Majstoravich, S. *et al.* Lymphocyte microvilli are dynamic, actin-dependent structures that do not require Wiskott-Aldrich syndrome protein (WASp) for their morphology. *Blood* **104,** 1396–1403 (2004).
41. von Andrian, U. H., Hasslen, S. R., Nelson, R. D., Erlandsen, S. L. & Butcher, E. C. A central role for microvillous receptor presentation in leukocyte adhesion under flow. *Cell* **82,** 989–999 (1995).
42. Singer, II. *et al.* CCR5, CXCR4, and CD4 are clustered and closely apposed on microvilli of human macrophages and T cells. *J. Virol.* **75,** 3779–3790 (2001).
43. Morgan, N. S., Heintzelman, M. B. & Mooseker, M. S. Characterization of myosin-IA and myosin-IB, two unconventional myosins associated with the *Drosophila* brush border cytoskeleton. *Dev. Biol.* **172,** 51–71 (1995).
44. Le Borgne, R. Regulation of Notch signalling by endocytosis and endosomal sorting. *Curr. Opin. Cell Biol.***18,** 213–222 (2006).
45. Emery, G. & Knoblich, J. A. Endosome dynamics during development. *Curr. Opin. Cell Biol.* **18,** 407–415 (2006).
46. Chhabra, E. S. & Higgs, H. N. The many faces of actin: matching assembly factors with cellular structures. *Nature Cell Biol.* **9,** 1110–1121 (2007).
47. De Joussineau, C. *et al.* Delta-promoted filopodia mediate long-range lateral inhibition in *Drosophila*. *Nature* **426,** 555–559 (2003).
48. Mullins, R. D., Heuser, J. A. & Pollard, T. D. The interaction of Arp2/3 complex with actin: nucleation, high affinity pointed end capping, and formation of branching networks of filaments. *Proc. Natl Acad. Sci. USA* **95,** 6181–6186 (1998).
49. Rohatgi, R., Milenkovic, L. & Scott, M. P. Patched1 regulates hedgehog signaling at the primary cilium. *Science* **317,** 372–376 (2007).
50. Kiprilov, E. N. *et al.* Human embryonic stem cells in culture possess primary cilia with hedgehog signaling machinery. *J. Cell Biol.* **180,** 897–904 (2008).
51. Ilagan, M. X. & Kopan, R. SnapShot: notch signaling pathway. *Cell* **128,** 1246 (2007).
52. Chen, H. & De Camilli, P. The association of epsin with ubiquitinated cargo along the endocytic pathway is negatively regulated by its interaction with clathrin. *Proc. Natl Acad. Sci. USA* **102,** 2766–2771 (2005).
53. Sigismund, S. *et al.* Clathrin-independent endocytosis of ubiquitinated cargos. *Proc. Natl Acad. Sci. USA* **102,** 2760–2765 (2005).
54. Imai, K., Nonoyama, S. & Ochs, H. D. WASP (Wiskott-Aldrich syndrome protein) gene mutations and phenotype. *Curr. Opin. Allergy Clin. Immunol.* **3,** 427–436 (2003).
55. Tanigaki, K. & Honjo, T. Regulation of lymphocyte development by Notch signaling. *Nature Immunol.* **8,** 451–456 (2007).
56. Osborne, B. A. & Minter, L. M. Notch signalling during peripheral T-cell activation and differentiation. *Nature Rev. Immunol.* **7,** 64–75 (2007).

METHODS

***Drosophila* genetics.** Stocks used in this study were: 1) y w; FRT80B (isogenized), 2) y w Ubx–FLP; RpS17[4] Ubi–GFP.nls FRT80B/TM3 Ser, 3) y w hs-FLP; UAS–N[ECN(NEXT)]/CyO; MKRS/TM2 (ref. 57), 4) y w; UAS-Arp3::GFP[58], 5) w; Wsp[3]/TM6B Tb[59], 6) Df(3R)3450/TM6B Tb, 7) y w; Arpc1[Q25St] FRT40A /CyO Kr-GAL4, UAS–GFP[60], 8) y w Ubx–FLP; Ubi–GFP.nls FRT40A/CyO, 9) y w hs-FLP; RpS17[4] Ubi–GFP FRT80B/ TM6B Tb, 10) y hs-FLP tubα1–GAL4 UAS–GFP.nls-6×Myc; tub–GAL80 RpS17[4] FRT80B/TM6B Tb, 11) w*; UAS–CD2::HRP/CyO (Bloomington Stock Center)[61], 12) w[1118]; neur[A101]–GAL4 Kg[V]/TM3 Sb[1] (Bloomington Stock Center)[62], 13) y w; numb[2] ck FRT40A/CyO[63], 14) y w ey-FLP; Ada[ear4] FRT40A/CyO y[+] (ref. 64), 15) w; FRT82B neur[1F65]/TMB6B Tb[65] 16) y w; sca[109–68]-GAL4 (ref. 66).

Rescue experiments were performed using the MARCM technique. Flies of genotype *y hs-FLP tubα1–GAL4 UAS–GFP.nls-6×Myc; UAS–Arp3::GFP/+; tub–GAL80 RpS17[4] FRT80B/ Arp3[515FC] FRT80B* were examined. The homozygous mutant bristles with longer and thicker appearance were differentiated from the short and thin *RpS17[4] (Minute* phenotype) bristles.

Epistasis analysis of *Arp3* with the ligand-independent form of Notch[57], N^{ECN} was performed by examining flies of the genotype *y w Ubx–FLP; sca[109–68]-GAL4/ UAS-N[ECN]; y[+] w[+] FRT80B/mwh Arp3[83F] FRT80B. Arp3* follicle cell clones in egg chambers were generated by heat-shocking virgin females of genotype *y w hs-FLP/+; FRT80B Arp3[515FC]/ RpS17[4] Ubi–GFP FRT80B* for 90 min at 38 °C for 3 consecutive days. Ovaries of heat-shocked females were dissected after 2–3 days of mating on medium supplemented with yeast.

The wing-disc signal-sending cell assay was performed as described previously[67,68] and flies of the genotype *y w hs-FLP UAS–GFP.CD8; tub–GAL80 FRT40A/ Arpc1 FRT40A; tub–GAL4/ UAS-Dl* were examined.

Immunohistochemistry. For conventional immunostaining, ovaries, wing discs from third instar larvae or pupal nota were dissected in PBS and fixed with 4% formaldehyde for 20 min. The samples were then permeabilized in PBS + 0.2% Triton X-100 (PBST) for 20 min and blocked with 5% normal donkey serum in PBST for 1 h. Samples were incubated with primary antibodies at 4 °C overnight. The following primary antibodies were used: chicken anti-GFP (1:2,000, Abcam), mouse anti-Cut (1:500; 2B10; Developmental Studies Hybridoma Bank, University of Iowa (DSHB))[69], rat anti-ELAV (1:200; 7E8A10; DSHB)[70], guinea pig anti-Sens (1:1,000; ref 71), mouse anti-Dl[ECD] (1:1,000; C594.9B; DSHB)[72], guinea pig anti-Delta (1:3,000; M. Muskavitch and A. L. Parks)[73], mouse anti-Fasciclin III (1:10; 7G10; DSHB)[74], mouse anti-Hnt (1:10; 1G9; DSHB)[75], Alexa Fluor 488- and 546-conjugated phalloidin (1 unit per reaction, Invitrogen), rabbit anti-Dlg (1:1,000; P. Bryant)[76], rat anti-Myo1B (1:500; M.S. Mooseker)[77]. The following antibodies were used in the experiments included in the Supplementary Information: rabbit anti-Numb (1:1,000; Y. N. Jan)[78], rabbit anti-Neuralized (1:600; E. C. Lai)[65], rat anti-*D*E-Cadherin (1:1,000, DCAD2, DSHB)[79], rabbit anti-Rab5 (1:200; M. González Gaitán)[80], rabbit anti-Rab11 (1:1,000, D. F. Ready)[81], guinea pig anti-Spinster/Benchwarmer (1:100; G. W. Davis)[82], guinea pig anti-Hrs-FL (1:600; ref. 83).The samples were then incubated with Cy3- and/or Cy5-conjugated affinity purified donkey secondary antibodies (1:500; Jackson ImmunoResearch Laboratories). Images were captured using an LSM510 confocal microscope and Leica TCS SP5 confocal microscope. Images were processed with Amira 5.0.1 and Adobe PhotoShop 7.0.

Transmission electron microscopy (TEM). To identify the pIIa-pIIb cells, we used flies of the following genotype: *UAS–CD2::HRP; neur[A101]-GAL4* (ref. 61). In this genotype the HRP-labelled cell membranes correspond to pIIa-pIIb at the 16–18 h APF time-point, as *neur[A101]-GAL4* drives expression of the CD2::HRP in the SOP and its progeny. To identify the SOP progeny in *Arp3* mutant clones for TEM analysis, we examined the flies with the genotype *y w Ubx–FLP;UAS–-CD2::HRP; Arp3[515FC] FRT80B neur[A101]-GAL4/ arm-lacZ M(3) tub–GAL80 FRT80B* in which the CD2::HRP is activated only in *Arp3* mutant SOP progeny.

HRP label was visualized by TEM as described previously[84] except for the following modifications: the pupal thorax was dissected at 18 h APF. After amplification and visualization of the HRP signal under a dissecting microscope, the tissues were fixed[85] to preserve the actin filament structures. The tissues were then processed for TEM using microwave irradiation with PELCO BioWave equipped with PELCO Cold Spot and Vacuum System. Serial sections (60 nm) were cut and post-stained with Reynold's lead citrate, and examined with a JEOL transmission electron microscope (JEOL 1010). The serial sections were labelled on the basis of their depth from the first electron micrograph that shows the most apical portion of HRP labelled SOP microvilli.

Immunoelectron microscopy of phalloidin. To label actin, the pupal thorax was dissected at 18 h APF, fixed in 1% glutaraldehyde in 0.1M PB pH 7.2 for 1.5 h, permeabilized in 0.1% Triton PBS for 5 min, labelled with biotin-XX phalloidin (3 units; Invitrogen) in PBS for 30–35 min. Samples were then incubated in streptavidin-HRP in TNT buffer (1:100; Sigma). To develop enzyme activity, we used a procedure described previously[84].

Delta endocytosis and pulse-chase assay. The endocytosis and pulse-chase assays were modified from previous reports[86,87]. Pupae were partially dissected in Schneider's medium at 18 h APF by making an incision along the dorsal side, and the internal tissues were washed out. The 'empty' pupal case was incubated with the supernatant of monoclonal antibody mouse anti-Delta[ECD] (1:10; C594.9B; DSHB)[72] for 15–20 min on ice in Schneider's medium supplemented with 25 μg ml^{-1} of 20-hydroxy-ecdysone (Sigma). The tissue was washed three times by medium changes. For the Delta pulse-chase assay the pupal cases were incubated at 25 °C for different time periods (0, 30 and 60 min) in Schneider's medium supplemented with 5 μg ml^{-1} of 20-hydroxy-ecdysone. For the endocytosis assay, the pupal cases were incubated in pre-warmed Schneider's medium supplemented with 5 μg ml^{-1} of 20-hydroxy-ecdysone at 34 °C in a water bath to inactivate the *shibire* gene in the negative control *shi[ts1]*. After incubation at 25 °C (pulse-chase assay) or 34 °C (endocytosis assay), the pupal cases were fixed for 20 min with 4% formaldehyde in Schneider's medium supplemented with 5 μg ml^{-1} of 20-hydroxy-ecdysone. The normal immunostaining protocol was then followed.

The following antibodies were used in the experiments in the pulse-chase co-labelling experiments in the Supplementary Information: rabbit anti-Rab5 (1:200; M. González Gaitán)[80], rabbit anti-Rab11 (1:1,000, D. F. Ready)[81], guinea pig anti-Spinster/Benchwarmer (1:100; G. W. Davis)[82], guinea pig anti-Hrs-FL (1:600; ref. 83).

Statistical analysis. Measurements of total number of Delta vesicles that traffic to the ARS 1 h after chase, and measurements of the total number of Delta vesicles endocytosed were analysed using a Student's *t*-test (***P <0.0001. Measurements of the ARS area were quantified using the Measure function of the ImageJ software. The measurements were analysed using a Student's *t*-test (***P <0.0001). For TEM, measurements of total number of microvilli in SOP and epithelial cells were quantified using ImageJ. The measurements were analysed using a Student's *t*-test (P <0.05).

The measurement of Delta colocalization with Rab5 and Rab11 as well as the determination of Delta, Rab11 and Rab5 signal intensities were quantified using the labelvoxel and materialstatistics functions in Amira 5.0.1. The measurements were analysed using a Student's *t*-test (*P =0.01).

Western blotting. For the Delta western blots, 50 embryos of the appropriate genotypes were collected at 0–13 h AEL and 13–19 hAEL and lysed in ice-cold filtered RIPA buffer (150 mM NaCl, 1.0% NP-40, 0.5% deoxycholic acid, 0.1% SDS, and 50 mM Tris, pH 8.0) with complete protease inhibitor cocktail (Roche). Lysates were suspended in equal volume of 3× Laemmli sample buffer in the absence of reducing agents, and proteins were resolved by SDS–PAGE. Delta was detected on a western blot using anti-Delta (mAb C594.9B) ascites fluid at 1:10,000. HRP-conjugated goat anti-mouse IgG (Jackson ImmunoResearch) was used at 1:10,000 and the blots were developed using Western Lightning chemiluminescent substrate (PerkinElmer LAS).

57. Struhl, G. & Greenwald, I. Presenilin-mediated transmembrane cleavage is required for Notch signal transduction in *Drosophila*. *Proc. Natl Acad. Sci.USA* **98,** 229–234 (2001).
58. Hudson, A. M. & Cooley, L. A subset of dynamic actin rearrangements in *Drosophila* requires the Arp2/3 complex. *J. Cell Biol.* **156,** 677–687 (2002).
59. Ben-Yaacov, S., Le Borgne, R., Abramson, I., Schweisguth, F. & Schejter, E. D. Wasp, the *Drosophila* Wiskott-Aldrich syndrome gene homologue, is required for cell fate decisions mediated by Notch signaling. *J. Cell Biol.* **152,** 1–13 (2001).
60. Zallen, J. A. *et al.* SCAR is a primary regulator of Arp2/3-dependent morphological events in *Drosophila*. *J. Cell Biol.* **156,** 689–701 (2002).
61. Watts, R. J., Schuldiner, O., Perrino, J., Larsen, C. & Luo, L. Glia engulf degenerating axons during developmental axon pruning. *Curr. Biol.* **14,** 678–684 (2004).

DOI: 10.1038/ncb1888

62. Lai, E. C. & Rubin, G. M. neuralized functions cell-autonomously to regulate a subset of notch-dependent processes during adult *Drosophila* development. *Dev. Biol.* **231,** 217–233 (2001).
63. Frise, E., Knoblich, J. A., Younger-Shepherd, S., Jan, L. Y. & Jan, Y. N. The *Drosophila* Numb protein inhibits signaling of the Notch receptor during cell–cell interaction in sensory organ lineage. *Proc. Natl Acad. Sci. USA* **93,** 11925–11932 (1996).
64. Berdnik, D., Torok, T., Gonzalez-Gaitan, M. & Knoblich, J. A. The endocytic protein α-Adaptin is required for numb-mediated asymmetric cell division in *Drosophila*. *Dev. Cell* **3,** 221–231 (2002).
65. Lai, E. C., Deblandre, G. A., Kintner, C. & Rubin, G. M. *Drosophila* neuralized is a ubiquitin ligase that promotes the internalization and degradation of Delta. *Dev. Cell* **1,** 783–794 (2001).
66. Manning, L. & Doe, C. Q. Prospero distinguishes sibling cell fate without asymmetric localization in the *Drosophila* adult external sense organ lineage. *Development* **126,** 2063–2071 (1999).
67. Wang, W. & Struhl, G. *Drosophila* Epsin mediates a select endocytic pathway that DSL ligands must enter to activate Notch. *Development* **131,** 5367–5380 (2004).
68. Tien, A. C. *et al.* Ero1L, a thiol oxidase, is required for Notch signaling through cysteine bridge formation of the Lin12-Notch repeats in *Drosophila melanogaster*. *J. Cell Biol.* **182,** 1113–1125 (2008).
69. Blochlinger, K., Bodmer, R., Jan, L. Y. & Jan, Y. N. Patterns of expression of cut, a protein required for external sensory organ development in wild-type and cut mutant *Drosophila* embryos. *Genes Dev.* **4,** 1322–1331 (1990).
70. Robinow, S. & White, K. Characterization and spatial distribution of the ELAV protein during *Drosophila melanogaster* development. *J. Neurobiol.* **22,** 443–461 (1991).
71. Nolo, R., Abbott, L. A. & Bellen, H. J. Senseless, a Zn finger transcription factor, is necessary and sufficient for sensory organ development in *Drosophila*. *Cell* **102,** 349–362 (2000).
72. Fehon, R. G. *et al.* Molecular interactions between the protein products of the neurogenic loci Notch and Delta, two EGF-homologous genes in *Drosophila*. *Cell* **61,** 523–534 (1990).
73. Parks, A. L., Klueg, K. M., Stout, J. R. & Muskavitch, M. A. Ligand endocytosis drives receptor dissociation and activation in the Notch pathway. *Development* **127,** 1373–1385 (2000).
74. Patel, N. H., Snow, P. M. & Goodman, C. S. Characterization and cloning of fasciclin III: a glycoprotein expressed on a subset of neurons and axon pathways in *Drosophila*. *Cell* **48,** 975–988 (1987).
75. Yip, M. L., Lamka, M. L. & Lipshitz, H. D. Control of germ-band retraction in *Drosophila* by the zinc-finger protein HINDSIGHT. *Development* **124,** 2129–2141 (1997).
76. Woods, D. F. & Bryant, P. J. The discs-large tumor suppressor gene of *Drosophila* encodes a guanylate kinase homolog localized at septate junctions. *Cell* **66,** 451–464 (1991).
77. Morgan, N. S., Heintzelman, M. B. & Mooseker, M. S. Characterization of myosin-IA and myosin-IB, two unconventional myosins associated with the *Drosophila* brush border cytoskeleton. *Dev. Biol.* **172,** 51–71 (1995).
78. Rhyu, M. S., Jan, L. Y. & Jan, Y. N. Asymmetric distribution of numb protein during division of the sensory organ precursor cell confers distinct fates to daughter cells. *Cell* **76,** 477–491 (1994).
79. Oda, H., Uemura, T., Harada, Y., Iwai, Y. & Takeichi, M. A *Drosophila* homolog of cadherin associated with armadillo and essential for embryonic cell–cell adhesion. *Dev. Biol.* **165,** 716–726 (1994).
80. Wucherpfennig, T., Wilsch-Brauninger, M. & Gonzalez-Gaitan, M. Role of *Drosophila* Rab5 during endosomal trafficking at the synapse and evoked neurotransmitter release. *J. Cell Biol.* **161,** 609–624 (2003).
81. Dollar, G., Struckhoff, E., Michaud, J. & Cohen, R. S. Rab11 polarization of the *Drosophila* oocyte: a novel link between membrane trafficking, microtubule organization, and oskar mRNA localization and translation. *Development* **129,** 517–526 (2002).
82. Sweeney, S. T. & Davis, G. W. Unrestricted synaptic growth in spinster-a late endosomal protein implicated in TGF-β-mediated synaptic growth regulation. *Neuron* **36,** 403–416 (2002).
83. Lloyd, T. E. *et al.* Hrs regulates endosome membrane invagination and tyrosine kinase receptor signaling in *Drosophila*. *Cell* **108,** 261–269 (2002).
84. Larsen, C. W., Hirst, E., Alexandre, C. & Vincent, J. P. Segment boundary formation in *Drosophila* embryos. *Development* **130,** 5625–5635 (2003).
85. Maupin, P. & Pollard, T. D. Improved preservation and staining of HeLa cell actin filaments, clathrin-coated membranes, and other cytoplasmic structures by tannic acid-glutaraldehyde-saponin fixation. *J. Cell Biol.* **96,** 51–62 (1983).
86. Le Borgne, R. & Schweisguth, F. Unequal segregation of Neuralized biases Notch activation during asymmetric cell division. *Dev. Cell* **5,** 139–148 (2003).
87. Emery, G. *et al.* Asymmetric Rab 11 endosomes regulate Delta recycling and specify cell fate in the *Drosophila* nervous system. *Cell* **122,** 763–773 (2005).

nature cell biology

DOI: 10.1038/ncb1888

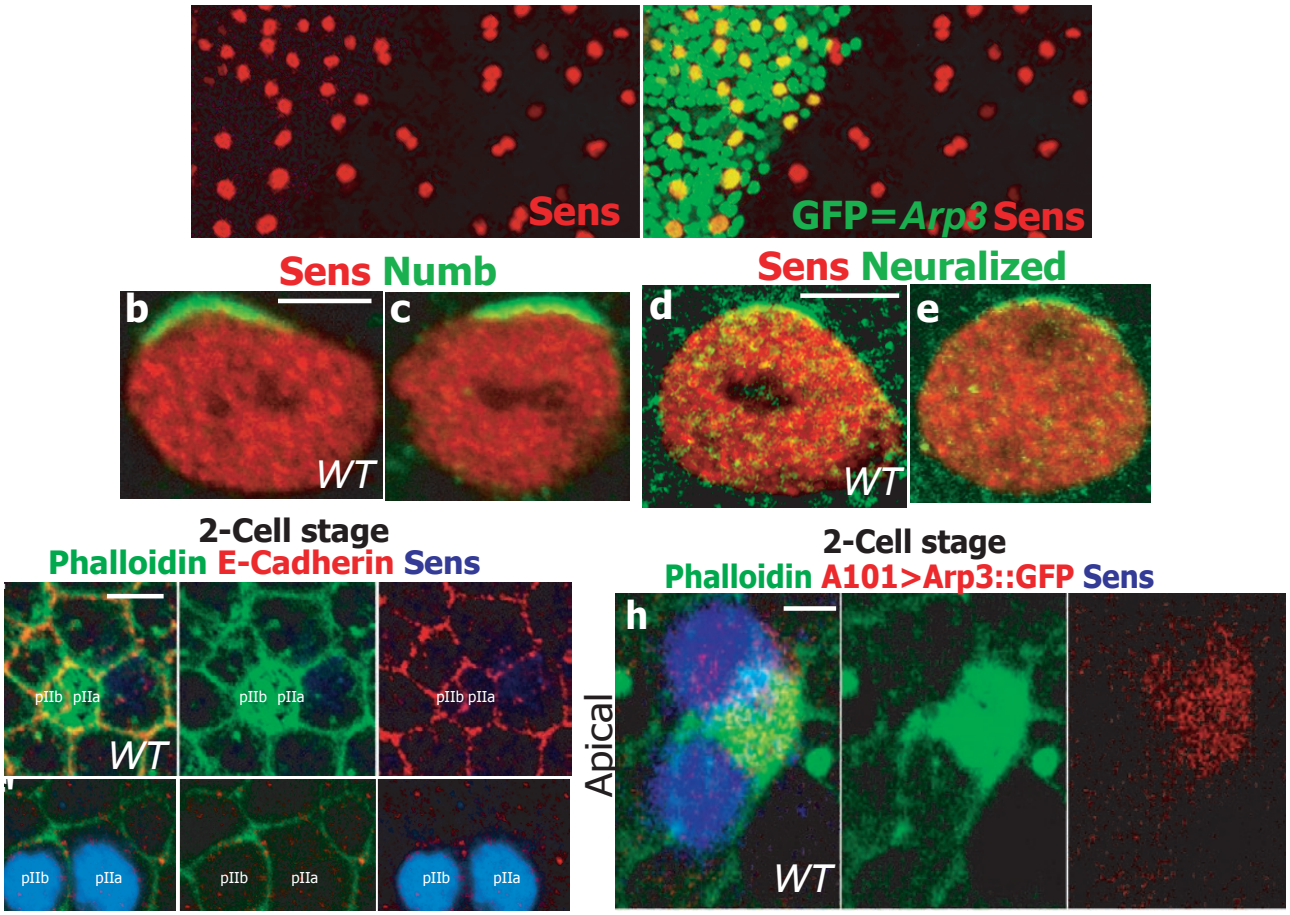

Figure S1 (**a** -**a'**) The SOPs are correctly specified in *Arp3*: (**a**) A projection of confocal sections along the XY-axis of a pupal notum at 17:30hr APF harboring *Arp3* clones marked by the presence of nuclear GFP (green) and immunostained for Sens (red) which marks the SOP and its progeny pIIa-pIIb. Note that SOPs are correctly specified in the mutant clones (green). (**b** -**e**) The segregation of asymmetric fate determinants is normal in *Arp3* mutant SOP: (**b** -**e**) Images showing a single confocal section along the XY-axis of a dividing SOP at 17:30hr APF of a *WT* or an *Arp3* pupal notum stained for asymmetric cell fate determinants (green) and Sens (red). Anterior side of the dividing SOP is oriented upwards in all these images. (**b**, **c**) Numb (green) segregates into the anterior side of the dividing SOP in both *WT* (**b**) and *Arp3* mutant clones (**c**), so that it is inherited into the anterior pIIb daughter. (**d**, **e**) Neuralized (green) segregates into the anterior side of the dividing SOP in both *WT* (d) and *Arp3* mutant clones (**e**), so that it is inherited into the anterior pIIb daughter. (**f** -**g'**) The ARS is formed only in the 2-cell stage: (**f**, **f'**) A confocal image of a single optical section along the XY-axis shows that the ARS forms above the pIIa-pIIb at the 2-cell stage. (**f**) *WT* pupal notum immunostained with phalloidin (green) reveals an apical (0.5 μm) actin enrichment, and this F-actin structure co-localizes with the apical stalk of the pIIa-pIIb cells marked by E-Cad (red). (**f'**) A basal section (~6 μm) of the sample shows the nuclei of the pIIa-pIIb cells marked with Sens (blue). (g, g') A confocal section along the XY-axis, showing immunostaining of *WT* pupal notum at the 1-cell stage with Sens (blue), phalloidin (green) and E-Cad (red). (**g**) The apical section (0.5 μm) reveals that the ARS has not yet formed at 1-cell stage. (**g'**) A basal section (6 μm) shows that the SOP, marked by Sens (blue) has not yet divided. F-actin (phalloidin–green) marks the cell membrane of the epithelial cells and SOP. (**h** -**h"**) Arp3 co-localizes with the ARS: (**h** -**h"**) Confocal images of a single optical section along the XY-axis (**h** -**h'**) and XZ-axis (**h"**) of pupal notum in which *UAS-Arp3-GFP* is expressed under the control of a *neuralized-GAL4* driver *A101-GAL4>Arp3::GFP* (red), immunostained with Sens (blue) and phalloidin (green) at the 2-cell stage. Scale bar: 10 μm in (a), 5 μm in (**f**- **g'**) and 2.5 μm in (**b**, **d**, **h**-**h"**).

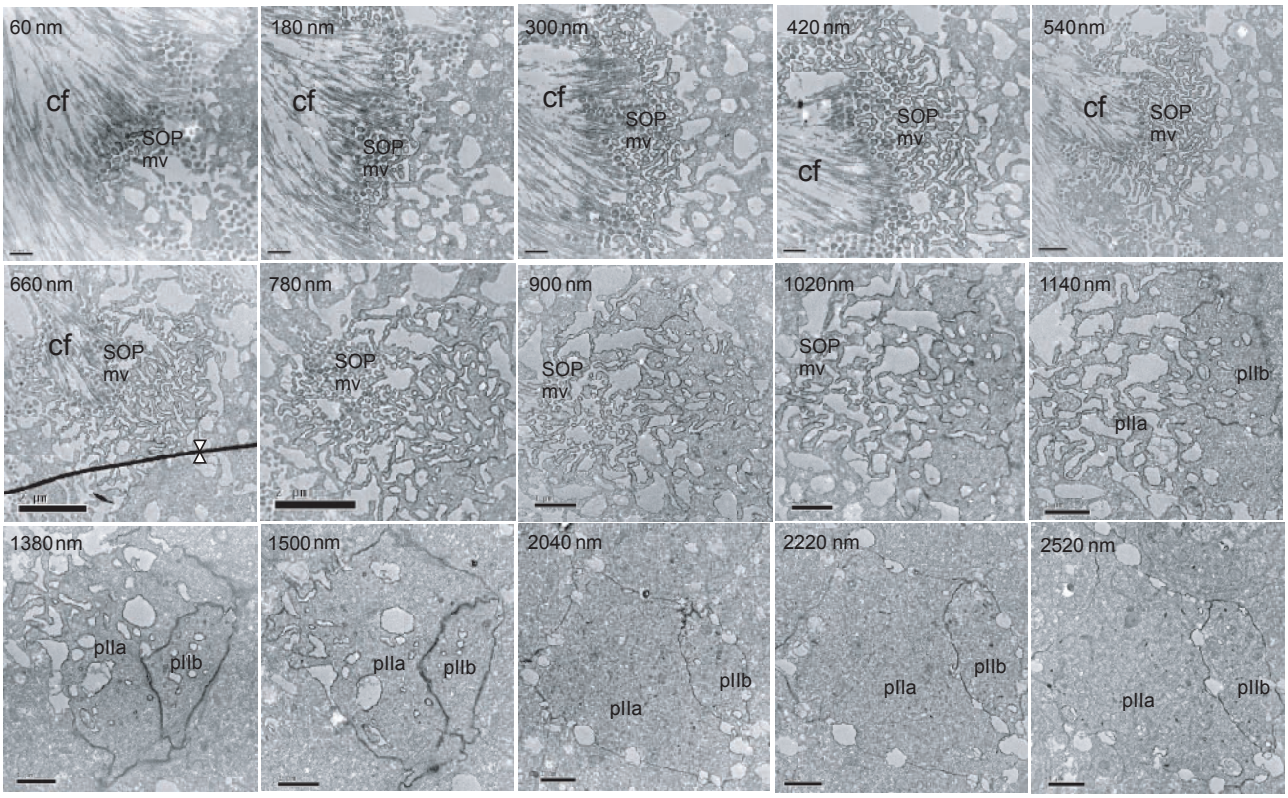

Figure S2 Transmission electron micrographs reveal the presence of finger-like projections on the apical surface of the pIIa-pIIb cells: Serial TEM micrographs of apical cross sections of pIIa-pIIb cells starting at 60 nm of the apical end through 2520 nm (basal end). Serial sections reveal the presence of numerous cross sections of finger-like projections, microvilli (mv) from 60 nm through 1020 nm. Sections from 1500 to 2520 nm show cell membrane outlines of pIIa-pIIb. The chitin fiber (cf) which assembles at the plasma membrane is a part of the apical extracellular matrix (cuticle). The dark line across 660nm with the double arrowhead is a section fold artifact.

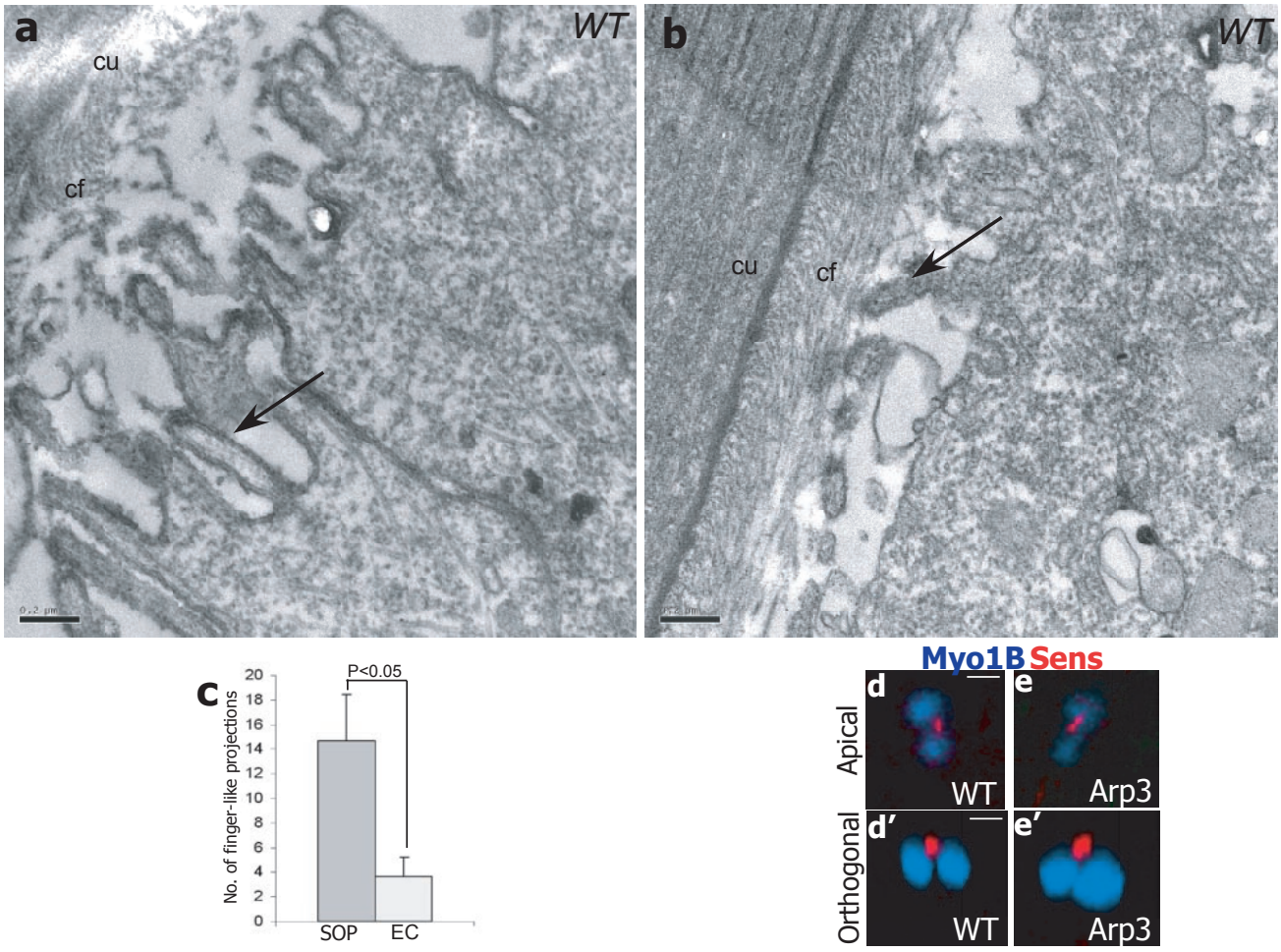

Figure S3 (**a** –**c**) The number of finger-like projections in pIIa-pIIb is significantly higher compared to those on epidermal cells: (**a**) TEM image along the XZ-axis of an SOP and (**b**) Epidermal cells at the 2-cell stage (**c**) A bar graph representing quantification of the number of finger-like projections in the epidermal cells versus the pIIa-pIIb cells. Three *WT* pIIa-pIIb pairs and six *WT* epidermal cells were used for this quantification. Arrows point to the finger-like projections. (**d** -**e'**) Microvilli marker Myo1B is correctly localized in *Arp3* mutant SOP progeny: (**d** -**e'**) Confocal images of single optical sections along the XY-axis (**d**, **e**) and the XZ-axis (**d'**, **e'**) depict immunostainings of *WT* (**d**, **d'**) and *Arp3* (**e**, **e'**) SOP progeny at the 2-cell stage, stained for Myo1B (red) and Sens (blue). Error bars indicate the SEM. Abbreviations: cuticle (cu), chitin fiber (cf). Scale bar: 0.2 µm in (**a**, **b**) and 5 µm in (**d**, **d'**).

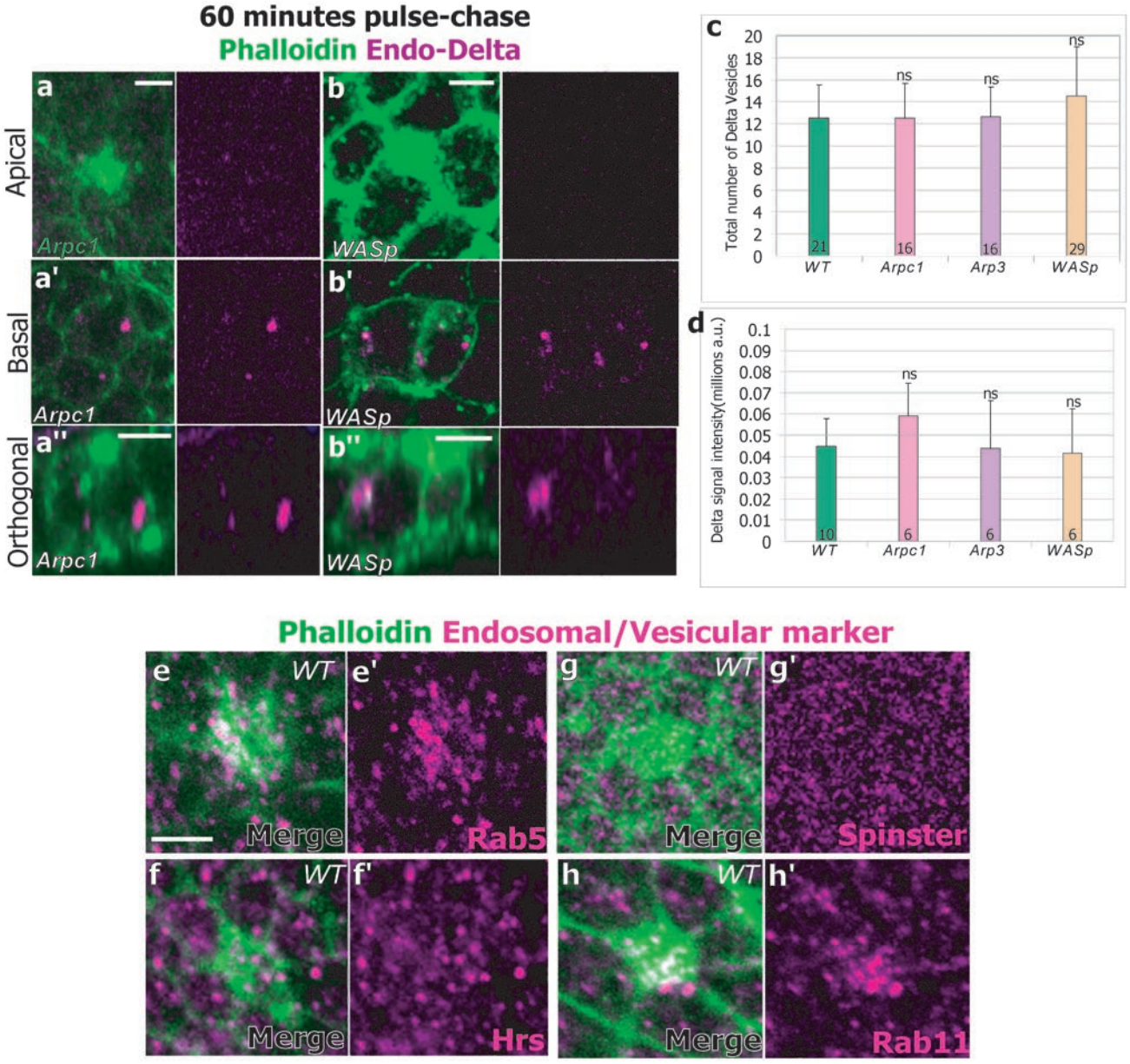

Figure S4 (**a**- **d**) Trafficking of endocytosed Delta traffics apically to the ARS after 60mins chase is compromised in *Arp2/3* and *WASp* mutants: (**a** -**b"**) Confocal images show a single section along the XY-axis (**a**, **a'**, **b**, **b'**) and XZ-axis (**a"**, **b"**) of SOP progeny at the 2-cell stage in *Arpc1* (**a**-**a"**) and *WASp* (**b**-**b"**) mutant during a 60 mins pulse-chase trafficking assay of internalized Delta–anti-Dl^{ECD} vesicles (magenta) with respect to the ARS stained by phalloidin (green). (**c**) A bar graph representing a quantification of the total number of internalized Delta vesicles which are present in the SOP progeny 60 mins after endocytosis. (**d**) A bar graph representing a quantification of the signal intensity of Delta immunostaining in the SOP progeny at 60 min chase. The number of SOP progeny (pIIa-pIIb) quantified per genotype is indicated in the bars. (**e –f'**) Early and recycling endosomes are enriched on the apical region of the ARS during fate specification: (**e** -**f'**) Confocal images of single Z-sections show immunostaining of ARS with phalloidin (green) and endosomal/vesicular markers (magenta) in *WT* pupal nota at the 2-cell stage. (**e**, **e'**) Rab5 (magenta) which marks the early endosome is enriched on the ARS (green). (**f**, **f'**) A subset of late endosomes marked by Hrs (magenta) do not show enrichment with respect to the ARS (green). (**g**, **g'**) The lysosomes marked by Spinster/ Benchwarmer (magenta) do not show enrichment relative to the ARS (green). (**e**, **e'**) Rab11 (magenta) which marks the recycling endosome is enriched with respect to the ARS (green). ns = not statistically significant. Error bars indicate SEM. Scale bar: **5** µm in (**a**, **b**, **a"**, **b"**) and 3.5 µm in (**e**).

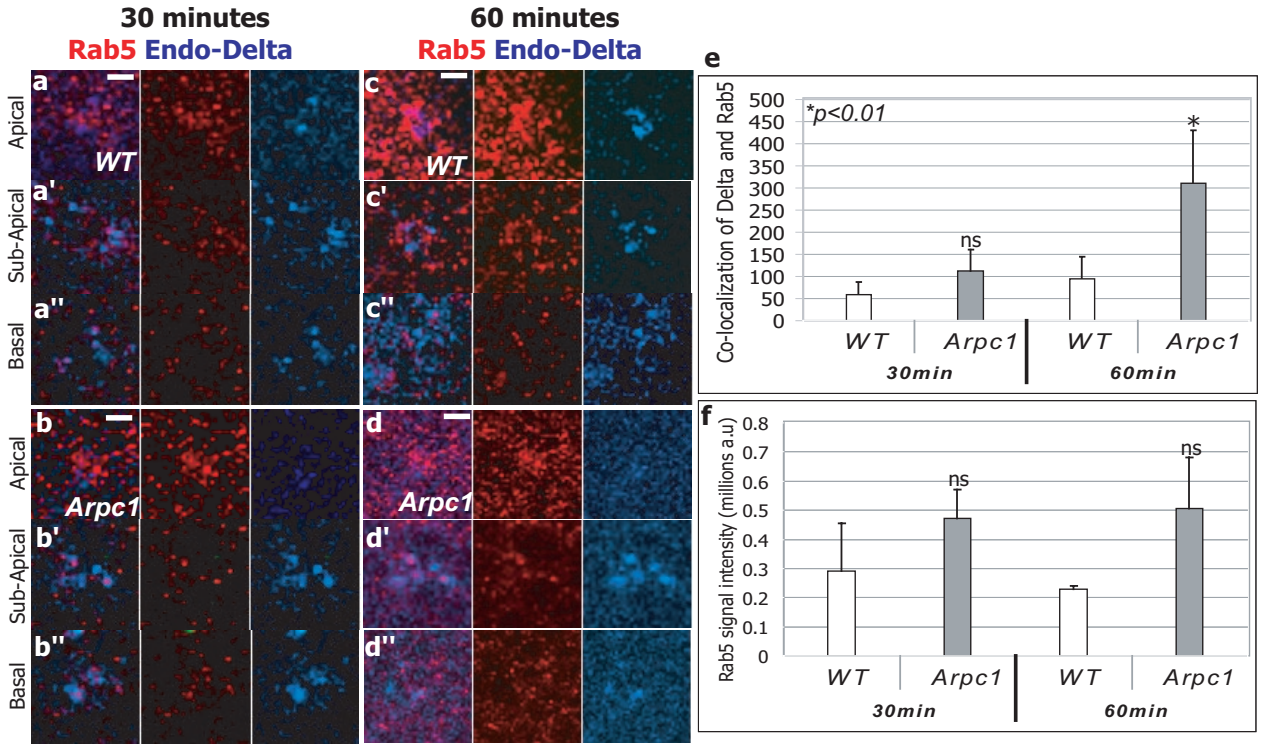

Figure S5 Pulse-chase trafficking of Delta with respect to the early endosomes (EE): Confocal images of single optical sections (**a**-**d"**) of SOP progeny at the 2-cell stage in *WT* (**a**-**a"**, **c**-**c"**) and *Arpc1* (**b**-**b"**, **d**-**d"**) after 30 mins (a-b") and 60 mins (c-**d"**) pulse-chase trafficking assays of internalized Delta–anti-DI^{ECD} (blue) with respect to the EE stained for Rab5 (red). (**a**-**d**) Apical sections (~0.5 µm) into the sample. (**a'**-**d'**) Sub-apical sections (~3 µm) into the sample. (**a"**-**d"**) Basal sections (~6 µm) into the sample. (**e**) A bar graph depicting co-localization intensity of Delta and Rab5 vesicles in arbitary units (a.u.). The measurements of signal intensities were analysed using a Student's t-test;*, p=0.01. Seven SOP progeny pairs were quantified per time point per genotype. (**f**) A bar graph depicting signal intensity of Rab5 vesicles in arbitary units (a.u.). The measurements of signal intensities were analysed using a Student's t-test;*, p=0.01. Seven SOP progeny pairs were quantified per time point per genotype. Abbreviation: ns = not statistically significant. Error bars indicate SEM. Scale bar: 3.5 µm.

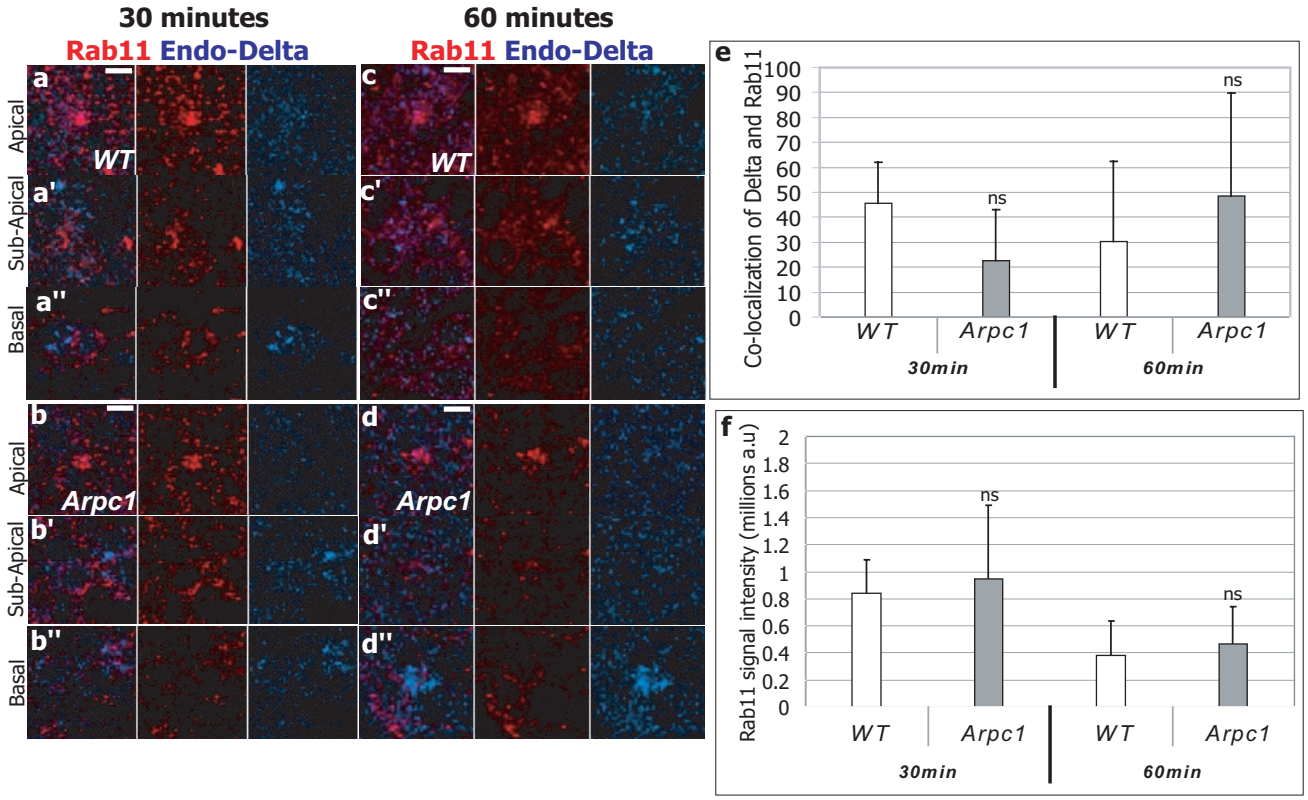

Figure S6 Pulse-chase trafficking of Delta with respect to the recycling endosomes (RE): Confocal images of single optical sections (**a**-**d”**) of SOP progeny at the 2-cell stage in *WT* (**a**-**a”**, **c**-**c”**) and *Arpc1* (**b**-**b”**, **d**-**d”**) after 30 mins (**a**-**b”**) and 60 mins (**c**-**d”**) pulse-chase trafficking assays of internalized Delta–anti-DI^{ECD} vesicles (blue) with respect to the RE stained for Rab11 (red). (**a**-**d**) Apical sections (~0.5 µm) into the sample. (**a’**-**d’**) Sub-apical sections (~3 µm) into the sample. (**a”**-**d”**) Basal sections (~6 µm) into the sample. (**e**) A bar graph depicting co-localization intensity of Delta and Rab11 vesicles in arbitrary units (a.u.). The measurements of signal intensities were analysed using a Student’s t-test;*, p=0.01. Seven SOP progeny pairs were quantified per time point per genotype. (**f**) A bar graph depicting signal intensity of Rab11 vesicles in arbitrary units (a.u.). The measurements of signal intensities were analysed using a Student’s t-test;*, p=0.01. Seven SOP progeny pairs were quantified per time point per genotype. Abbreviation: ns = not statistically significant. Error bars indicate SEM. Scale bar: 3.5 µm.

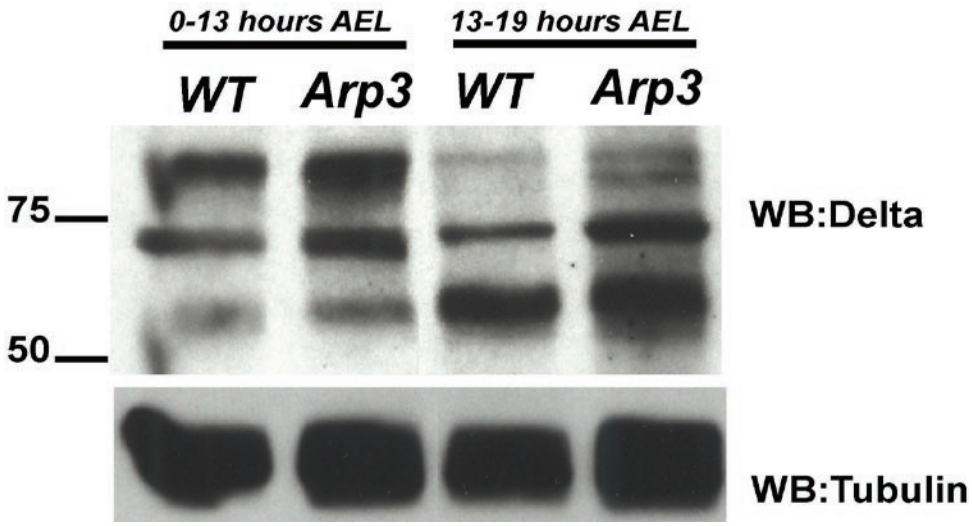

Figure S7 The processing of Delta in *Arp3* mutant embryos is unaffected: Western blotting analysis of *WT* and *Arp3* embryo lysates at 0-13hr AEL and 13-19hr AEL probed with mouse anti-Delta ascites fluid. At 0-13hr AEL note the presence of a 98 kDa band in *WT* and *Arp3* lanes. The Delta S isoform (68 kDa, is present at 0-13hr AEL but is weaker compared to the 98 kDa band. At 13-19hr AEL the 98 kDa band is much reduced in *WT* and *Arp3*. The Delta S isoform (68 kDa, arrow) is highly enriched at the 13-19 hr AEL time point in both *WT* and *Arp3* mutant. In the *Arp3* lane we sometimes observe a doublet at 98 kDa at 13-19hr AEL, but not consistently in various independent trials of the experiment.

Supplementary material:

Results:

Early and recycling endosomes are enriched on the apical region of the ARS during fate specification:

It has been proposed that Delta must be endocytosed and targeted to a specific endosomal compartment to become activated[1], possibly through a Rab11-positive recycling endosomal compartment[2, 3]. Based on our data, the ARS may have a role in these trafficking events. We therefore examined the co-localization of different endosomal compartments with respect to the ARS during cell fate specification. Immunostaining with endosomal and vesicular compartment markers including Rab5 (early endosomes, EE)[4], Rab11 (recycling endosomes, RE)[5], Hrs (late endosomes, LE)[6] and Spinster (lysosomes)[7, 8] revealed that EE and RE are enriched apically where they co-localize with the microvillar region of the ARS in the pIIa-pIIb at the 2-cell stage (Supplementary Fig. 4 e, e', h, h'). However, the LE and lysosomes are not enriched with respect to the ARS (Supplementary Fig. 4 g, g', f, f'). We find the localization of these endosomal and vesicular compartments are similar to *WT* in *Arp3, Arpc1* mutant pIIa-pIIb cells (data not shown).

Endosomal trafficking of Delta through the early endosomes (EE) and recycling endosomes (RE) during pIIa-pIIb fate specification:

To examine if Delta trafficking through the EE and RE is altered in mutants of the Arp2/3 complex, we performed pulse chase assays at 30 mins and 60 mins after

internalization (Supplementary Fig. 5, 6). We focused on these compartments as they were enriched on the ARS at the 2-cell stage (Supplementary Fig. 4 e, e', h, h'). With regard to the Rab5-positive EE compartment we find that there is no statistically significant difference of Delta co-localization with this compartment between *WT* and mutant at 30 mins post-internalization (Supplementary Fig. 5 a-b'', e). However, after 60 mins chase there seems to be a borderline significant increase in Delta vesicle co-localization to the Rab5 compartment (p=0.01, student's two-tailed test) in *Arpc1* mutants compared to *WT* (Supplementary Fig. 5 c-d'', e). We also assayed if the abundance of the EE is altered in the *Arpc1* mutant by quantifying the signal intensity of Rab5 immuno-staining in the *Arpc1* mutant pIIa-pIIb cells, 30 min and 60 mins after internalization, and we find that there is no significant difference (Supplementary Fig. 5 f).

Furthermore, we found that there is not a statistically significant difference of Delta trafficking with respect to the Rab11-positive RE at both 30 mins and 60 mins post internalization (Supplementary Fig. 6 a-d'', e). The distribution and abundance of the Rab11 compartment itself remains largely unaffected in the *Arpc1* mutants (Supplementary Fig. 6 f). In addition, when the pI cell divides, Emery et al (2005) have reported that Rab11 localizes asymmetrically to the pIIb cell[3]. We found that this asymmetric distribution of Rab11 to the pIIb compartment is unaffected in dividing pIs of *Arp3* mutants (data not shown).

Our hypothesis based on these results is that the primary defect in *Arp2/3* mutants is their inability to traffic Delta to the apical region of the ARS, and we consider this increased co-localization of Delta to the Rab5 compartment as a

secondary defect that seems to occur when the Delta vesicles do not arrive at their expected destination. The reason we favor this hypothesis is that the inability of Delta to cluster around the ARS and traffic apically seems to be a highly significant (Fig. 8g) defect as compared to a subtle increase in Delta co-localization to the Rab5 positive compartment (Supplementary Fig. 5e).

Delta processing is unaffected in *Arp3* mutants:

Wang and Struhl[1] have suggested that the internalization of Delta leads to a proteolytic cleavage in an unknown compartment. *Drosophila* full-length Delta (~98 kDa) is proteolytically processed into three different isoforms *in vivo*[9] and the short isoform Delta S (~68 kDa) may correspond to the activated form[1, 9]. During early stages of embryogenesis (0-6 hours after egg laying, hr AEL) the Delta S isoform is not generated[45]. At later developmental stages (13-24hr AEL) full-length Delta is much reduced, but the Delta S isoform is far more abundant[45]. To assay if lack of Arp2/3 function alters Delta processing we prepared lysates from *WT*, *Arp3* and *Arpc1* zygotic mutant embryos at two different developmental time periods, 0-13hr AEL and 13-19hr AEL, for western blot analysis. We find that processing of Delta is largely unaltered in *Arp3* embryos (Supplementary Fig. 7), suggesting that the processing of Delta may not depend on Arp2/3 function.